HHS Public Access

Author manuscript

Cell Rep. Author manuscript; available in PMC 2024 May 13.

Published in final edited form as:

Cell Rep. 2024 April 23; 43(4): 113984. doi:10.1016/j.celrep.2024.113984.

Acod1 expression in cancer cells promotes immune evasion through the generation of inhibitory peptides

James H. Schofield[1], **Joseph Longo**[2], **Ryan D. Sheldon**[3], **Emma Albano**[1], **Abigail E. Ellis**[3], **Mark A. Hawk**[1], **Sean Murphy**[1], **Loan Duong**[1], **Sharif Rahmy**[1], **Xin Lu**[1], **Russell G. Jones**[2], **Zachary T. Schafer**[1,4,*]

[1]Department of Biological Sciences, University of Notre Dame, Notre Dame, IN 46556, USA

[2]Department of Metabolism and Nutritional Programming, Van Andel Institute, Grand Rapids, MI 49503, USA

[3]Mass Spectrometry Core, Van Andel Institute, Grand Rapids, MI 49503, USA

[4]Lead contact

SUMMARY

Targeting programmed cell death protein 1 (PD-1) is an important component of many immune checkpoint blockade (ICB) therapeutic approaches. However, ICB is not an efficacious strategy in a variety of cancer types, in part due to immunosuppressive metabolites in the tumor microenvironment. Here, we find that αPD-1-resistant cancer cells produce abundant itaconate (ITA) due to enhanced levels of aconitate decarboxylase (Acod1). Acod1 has an important role in the resistance to αPD-1, as decreasing Acod1 levels in αPD-1-resistant cancer cells can sensitize tumors to αPD-1 therapy. Mechanistically, cancer cells with high Acod1 inhibit the proliferation of naive $CD8^+$ T cells through the secretion of inhibitory factors. Surprisingly, inhibition of $CD8^+$ T cell proliferation is not dependent on the secretion of ITA but is instead a consequence of the release of small inhibitory peptides. Our study suggests that strategies to counter the activity of Acod1 in cancer cells may sensitize tumors to ICB therapy.

Graphical Abstract

*Correspondence: zschafe1@nd.edu.

AUTHOR CONTRIBUTIONS

J.H.S., J.L., R.D.S., E.A., A.E.E., and M.A.H. conducted experiments, analyzed data, and interpreted results. S.M., L.D., S.R., and X.L. generated the PRs and PRp cell lines and assisted with isolation of T cells from mice. J.L., R.D.S., A.E.E., and R.G.J. were responsible for MS-based analysis. X.L., R.G.J., and Z.T.S. provided funding and supervision for the project. J.H.S. and Z.T.S. were responsible for conception/design of the project and wrote the manuscript with feedback from all other authors. Z.T.S. was responsible for overall study supervision.

SUPPLEMENTAL INFORMATION

Supplemental information can be found online at https://doi.org/10.1016/j.celrep.2024.113984.

DECLARATION OF INTERESTS

R.G.J. is a scientific advisor for Agios Pharmaceuticals and Servier Pharmaceuticals and is a member of the scientific advisory board of ImmunoMet Therapeutics.

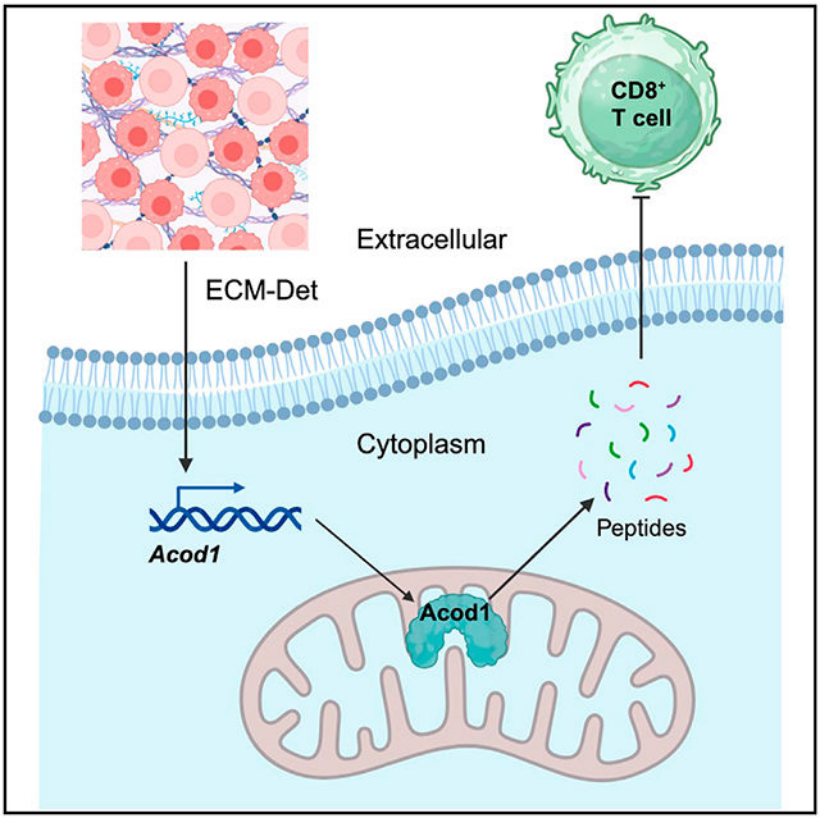

In brief

Schofield et al. report that cancer cells upregulate Acod1 as a survival strategy in response to αPD-1 therapy. Acod1^{hi} cancer cells secrete inhibitory peptides that block the activation of naive CD8^{+} T cells. Loss of Acod1 resensitizes resistant tumors to αPD-1 ICB.

INTRODUCTION

The exploitation of the immune system to target cancer using the immune checkpoint blockade (ICB) strategy has revolutionized cancer treatment in recent years.[1-3] More specifically, antibodies targeting programmed cell death protein 1 (PD-1) can dampen the natural resistance of cytotoxic CD8^{+} T cells toward host cells and lead to increased recognition and destruction of cancerous cells.[4] Use of this strategy has shown strong efficacy in patients with melanoma and non-small cell lung cancer.[5-7] Despite these exciting findings, many cancers are relatively insensitive (or entirely resistant) to αPD-1 (and other ICB) therapy.[8,9] For instance, αPD-1 therapies in castration-resistant prostate cancer (CRPC) have largely failed to demonstrate durable clinical response.[10,11] As such, there remains a significant need to better understand the molecular mechanisms that underlie the sensitivity (or insensitivity) of cancer cells to ICB therapy.

The tumor microenvironment (TME) has emerged as a key determinant of sensitivity to αPD-1 ICB therapy.[12] In particular, extracellular metabolites present in the TME can often function to drive the immune response to a variety of malignancies.[13-15] For

example, depletion of immunosuppressive metabolites within the TME reduces tumor size through enhancing the anti-tumor activity of cytotoxic $CD8^+$ T cells.[16,17] One metabolite that has recently garnered significant interest for its capacity to impact the immune response is itaconate (ITA). ITA is derived from the tricarboxylic acid (TCA) cycle through the enzymatic action of *cis*-aconitate decarboxylase 1 (Acod1, also known as Irg1), which catalyzes the decarboxylation of *cis*-aconitate to form ITA.[18] ITA has putative anti-inflammatory properties and has been revealed by multiple studies to have a significant role in regulating macrophage polarization.[19-25] Relatedly, *Acod1* expression appears to be upregulated under inflammatory stress in macrophages, monocytes, and dendritic cells.[26,27] More recently, ITA has been discovered to have some capacity to regulate additional cell types, including neutrophils,[28,29] T cells,[30,31] and epithelial cells.[32] Despite these important findings, the underlying mechanisms by which *Acod1* expression and ITA production alter behavior and function in other cell types remain inadequately characterized.

Here, we report that ICB-resistant cancer cells produce high amounts of ITA due to a significant elevation in Acod1 levels. This increase in Acod1 has a significant impact on ICB resistance as previously insensitive tumors, engineered to be deficient in Acod1, regain sensitivity to αPD-1 therapy. Mechanistically, cancer cells with high levels of Acod1 release factors into the extracellular space that block the activation and proliferation of $CD8^+$ T cells. Surprisingly, the inhibition of $CD8^+$ T cell proliferation is not due to ITA secretion by Acod1-high cancer cells. Instead, these cells produce small peptides that have the capacity to block $CD8^+$ T cell proliferation. Taken together, our data suggest that strategies aimed at countering Acod1-mediated generation of small peptides in cancer cells may be efficacious in sensitizing tumors to ICB therapy.

RESULTS

ITA is produced at high levels by ICB-resistant prostate cancer cells

In order to investigate links between changes in cancer cell metabolism and immune modulation, we utilized cell lines generated from a Probasin-driven *PB-Cre*$^+$ *Smad4*$^{L/L}$/*Pten*$^{L/L}$/*Tp53*$^{L/L}$ mouse model of CRPC.[33] Tumors from these mice respond to αPD-1 ICB monotherapy and were used to derive a cell line for use in subsequent analyses (PPS-6239).[34] To generate ICB-resistant variants of PPS-6239 cells, these cells were injected into syngeneic hosts, allowed to form tumors, treated with αPD-1, and isolated from rare tumors that were not responsive to ICB monotherapy (Figure S1). The resulting cells, termed PPS-PD1R, were resistant to αPD-1 monotherapy after injection into syngeneic hosts.[34] For the sake of simplicity, we will here-after refer to the PPS-6239 cells as PRs (for prostate sensitive) and the PPS-PD1R cells as PRp (for prostate PD-1 resistant).

Having established these isogenic cell lines, we first sought to characterize metabolic changes associated with differing sensitivity to αPD-1 ICB therapy. We began this analysis by assessing mitochondrial metabolism in the PRs and PRp cell lines. Motivated by our recent findings demonstrating that detachment from extracellular matrix (ECM) can trigger mitophagy (the degradation of mitochondria in autophagosomes) in a fashion that causes cell death,[35-37] we assessed mitochondrial abundance in ECM-detached conditions. ICB-sensitive PRs cells indeed display lower mitochondrial mass during ECM detachment as

evidenced by the reduction in the MitoTracker signal (Figures 1A-1C) and diminished levels of mitochondrial proteins (Figure S2A). In contrast, ICB-insensitive PRp cells maintain mitochondrial integrity in ECM-detached conditions and display increased anchorage-independent growth (Figures 1A-1C, S2A, and S2B), suggesting that they are better able to successfully adapt to ECM detachment in a fashion that promotes tumor progression and/or metastasis.[38,39]

Given these results, we reasoned that maintenance of mitochondrial abundance during ECM detachment may cause ICB-insensitive cells to utilize distinct metabolic pathways. To better understand metabolic differences between the ICB-insensitive and -sensitive cells, we conducted intracellular metabolomic profiling of PRs and PRp cells cultured in ECM-detached conditions. Surprisingly, ITA was the most significantly elevated metabolite in the PRp cells compared to the PRs cells (Figure 1D). Given the abundance of ITA produced in PRp cells, we next sought to determine if the elevated levels of ITA were synthesized by flux originating from glucose or glutamine, two carbon sources widely utilized by cancer cells.[40] Indeed, labeling cells with [U-^{13}C]glucose (Figure 1E) or [U-^{13}C]glutamine (Figure 1F) revealed that PRp cells direct carbon flux from both nutrient sources into elevated production of ITA at a level that is significantly higher than PRs cells.

Acod1 levels are elevated in ICB-resistant cells

As mentioned previously, the majority of studies on ITA have been conducted on cells of the monocyte-macrophage lineage, and we were therefore surprised by its detection in prostate cancer cells.[41-43] We next sought to investigate if the changes in ITA in PRp cells are associated with changes in Acod1, the enzyme responsible for ITA production (see diagram in Figure 2A).[18] Indeed, we found that Acod1 protein levels are elevated in the PRp cells when compared to PRs cells and that ECM detachment promotes an increase in Acod1 levels in both cell lines (Figure 2B). Furthermore, expression of the *Acod1* transcript mirrored the protein data, as mRNA levels are higher in PRp cells compared to PRs cells and similarly stimulated by ECM detachment (Figure 2C). These findings are not limited to the PRs and PRp cell lines, as we found that PC3 cells, a well-established human prostate cancer cell line, have discernable levels of ACOD1 protein that are increased as a consequence of ECM detachment (Figure S3A). We also expanded our analysis of ACOD1 protein levels into other cancer cell lines of diverse origin, and we found robust levels of ACOD1 protein in the GCT (derived from a fibrous histiocytoma) and MDA-MB-436 (derived from a pleural effusion in a patient with triple-negative breast cancer) cell lines (Figure S3B). Given that Acod1 is known to localize to the mitochondria,[44] we reasoned that the elevation in Acod1 levels seen in PRp cells may be, at least partially, due to the deficient capacity to induce mitophagy during ECM detachment in these cells (Figures 1A-1C, S2A, and S2B). In support of this possibility, treatment of ECM-detached PRp cells with the mitochondrial uncoupler carbonyl cyanide *m*-chlorophenyl hydrazone (CCCP), a well-described inducer of mitophagy, resulted in a decrease in both Acod1 and Sdhb, a TCA cycle protein used as a positive control for CCCP treatment (Figure 2D).

We next examined how Acod1 levels are regulated in prostate cancer cells. Previous studies have determined that diminished integrin function in epithelial cells during separation from

the ECM activates the nuclear factor κB (NF-κB) signaling pathway.[35,45] Relatedly, *Acod1* expression has previously been found to be regulated by NF-κB signaling.[46] Thus, we assessed the contribution of NF-κB signaling to the increase in Acod1 levels observed in ECM detachment. Indeed, treatment of detached PRp cells with BAY1170-82, an NF-κB inhibitor, caused a significant downregulation of both Acod1 protein (Figure 2E) and *Acod1* mRNA expression (Figure S3C). We therefore conclude that NF-κB signaling contributes to the ECM-detachment-induced Acod1 increase in prostate cancer cells.

Acod1 dictates sensitivity to αPD-1 ICB *in vivo*

Given the elevation in Acod1 levels in the PRp cells, we were interested in whether Acod1 contributes to the insensitivity of PRp tumors to αPD-1 monotherapy (see schematic in Figure 3A). As such, we engineered PRp cells to be deficient in Acod1 (Figure 3B) and then inoculated control (PRp Scr [scramble gRNA]) or Acod1 knockout (PRp Acod1 KO) cells subcutaneously into male C57BL/6 mice. After 11 days of tumor growth, we subjected these mice to αPD-1 monotherapy (or control immunoglobulin G [IgG]), measured the tumor volumes over time, and collected tumors at the endpoint (day 29) for immunophenotyping analysis. We found that while loss of Acod1 alone did not alter the growth of PRp tumors *in vivo*, it did restore sensitivity of these tumors to αPD-1 ICB therapy (Figure 3C). To gain insight into how tumor growth was restricted in these tumors generated from Acod1-deficient cells, we characterized the immune infiltration in the tumors at the time of harvest (see schematic in Figure S4A). Acod1 loss alone was not sufficient to cause an increase in the total immune infiltrate within the tumor in either the IgG or the αPD-1 treatment (Figure S4C). Moreover, neither KO of Acod1 nor administration of αPD-1 monotherapy altered the intratumoral percentage of $CD4^+$ T cells (Figures 3D and S4B). However, the tumors generated from PRp cells deficient in Acod1 had a marked increase in the number of $CD8^+$ T cells (Figures 3E and S4B). Tumor regression following therapeutic αPD-1 is dependent upon pre-existing $CD8^+$ T cells within the tumor, thus emphasizing the importance of increased $CD8^+$ T cell infiltrate in the Acod1-deficient tumors.[47]

To gain a better understanding of the functional changes caused by the Acod1-mediated elevation in $CD8^+$ T cells, we performed immunohistochemistry for granzyme B (GzmB) on the tumors from Figure 3C. GzmB is a serine protease released by $CD8^+$ T cells during their attack on cancer cells and represents an important mechanism of T cell-mediated killing of tumor cells.[48,49] Immunofluorescent staining in PRp tumors showed that loss of Acod1 alone was not sufficient to increase GzmB produced by T cells within the TME (Figures 3F and 3G). However, the absence of Acod1 in PRp tumors, combined with αPD-1 treatment, enhances GzmB production within the TME. As a result, we also observed elevated tumor cell death as measured by TUNEL+ (Figures 3F and 3G). We therefore conclude that the reduction of Acod1 in cancer cells increases sensitivity to αPD-1 monotherapy by elevating cytotoxic $CD8^+$ T cell numbers, which are better capable of killing tumor cells.

Conditioned media (CM) from cancer cells with high levels of Acod1 inhibit naive $CD8^+$ T cell activation and proliferation

Given the increased number of $CD8^+$ T cells in tumors derived from cells engineered to be deficient in Acod1, we reasoned that Acod1 may facilitate the release of immunomodulatory

factors from cancer cells. More specifically, cancer cells that form αPD-1-resistant tumors have been shown to release immunosuppressive factors that can inhibit the transition of $CD8^+$ T cells from a naive to an activated state,[50] which could alter the sensitivity of tumors to αPD-1 ICB monotherapy. We therefore employed a T cell activation assay to investigate how PRp cell CM impacted $CD8^+$ T cell activation and proliferation. Indeed, αCD3/CD28-stimulated $CD8^+$ cells activated in CM generated from PRp cells had substantially reduced proliferation, as evidenced by reduced EdU incorporation (Figure 4A) and violet proliferation dye 450 dilution both (Figure 4B), whereas there was no deficit in proliferation of T cells activated in CM generated from PRs cells (Figures 4A and 4B). In addition, T cell activation, as measured by cell surface levels of CD44 and CD25, was also dampened when naive $CD8^+$ T cells were activated in PRp (but not PRs) CM (Figures 4C and 4D). Given that Acod1 levels are high in PRp cells and that reducing Acod1 sensitized PRp tumors to αPD-1 monotherapy, we posited that Acod1 may regulate the ability of PRp cells to block the activation and proliferation of $CD8^+$ T cells. Additionally, previous work has demonstrated that PC3 cells (which have detectable ACOD1 levels), but not DU-145 cells (which do not have detectable ACOD1) (Figure S3A), can secrete factors that modulate the activity of T cells.[50] We first confirmed that, as expected, our PRp Acod1 KO cells lost the capacity to both produce and secrete ITA (Figures S5A and S5B). To interrogate the contribution of Acod1 to the inhibitory phenotype, CM was generated from these cell lines and used in the T cell proliferation/activation assays described above. Interestingly, CM generated from PRp Acod1 KO cells was unable to inhibit $CD8^+$ T cell proliferation (Figures 4E and 4F). Loss of Acod1 also increased activation markers (CD44/CD25) in T cells cultured in PRp Acod1 KO CM compared to PRp Scr CM (Figures 4G and 4H). Taken together, these data suggest that Acod1 regulates the secretion of inhibitory factors from cancer cells that negatively impact both activation and proliferation of $CD8^+$ T cells.

Acod1-mediated inhibition of $CD8^+$ T cell proliferation/activation is independent of extracellular ITA

As previously mentioned, the only documented role (to our knowledge) for Acod1 is catalyzing the decarboxylation of *cis*-aconitate to form ITA. Acod1-mediated ITA can be secreted into the extracellular space[18,51] and, despite its hydrophobic nature, can cross the plasma membrane and be utilized by recipient cells.[52] In addition to the known immunomodulatory roles of ITA in macrophages,[46] recent studies have examined a role for ITA in the regulation of T cell proliferation and differentiation.[30,31,53] We thus posited that secretion of extracellular ITA by cancer cells expressing Acod1 can result in the inhibition of $CD8^+$ T cell proliferation/activation. To test this hypothesis, we first activated $CD8^+$ T cells in media supplemented with increasing concentrations of exogenous ITA. Our choice of concentrations to test was informed by previous research assessing the abundance of extracellular ITA in different settings.[51] Surprisingly, exogenous ITA supplementation did not impact the proliferation of $CD8^+$T cells except at very high (10 mM) concentrations (Figure 5A). Additionally, there was no impact of ITA on the percentage of activated $CD8^+$ T cells at any of the concentrations tested (Figures 5B and 5C); however, a slight decrease in CD25 (but not CD44) on a per-cell basis was noted with increasing ITA concentrations. In addition to examining activation and proliferation of $CD8^+$ T cells, we also measured the effect of exogenous ITA supplementation on cytokine production. We

observed a concentration-dependent decrease in interferon gamma (IFN-γ) production with increasing concentrations of ITA (Figure 5D) but observed little to no effect on GzmB production (Figure S5C). As such, our data show that ITA does not phenocopy the effects of PRp CM on $CD8^+$ T cell proliferation or activation but that it impairs IFN-γ production by $CD8^+$ T cells. Lastly, we thought it prudent to quantitatively determine the concentration of ITA in the CM generated from the PRs and PRp cell lines. As expected, we did see a significant elevation in the abundance of ITA secreted by PRp (compared to PRs) cells (Figure 5E). However, the concentration of ITA in PRp CM topped out at slightly over 500 nM, far below the concentrations (10 mM) at which we observed effects of ITA on $CD8^+$ T cell proliferation. Taken together, our data suggest that secretion of ITA is not responsible for the capacity of CM collected from Acod1-expressing cancer cells to antagonize $CD8^+$ T cell proliferation and activation.

Acod1 regulates the secretion of immunomodulatory small peptides

Our data demonstrate that cancer cells are capable of secreting factors that inhibit $CD8^+$ T cells through a mechanism dependent on Acod1, but independent of extracellular ITA (see Figures 4 and 5). As such, we were interested in determining the identity of the secreted factor (or factors) that impacts $CD8^+$ T cells. To do so, we first boiled CM from PRs or PRp cells to assess whether something proteinaceous was involved in the inhibition of $CD8^+$ T cells. Interestingly, the capacity of CM from PRp cells to inhibit the proliferation of $CD8^+$ T cells was maintained after boiling (Figures 6A and S6A), suggesting that heat-labile proteinaceous factors were not responsible for the inhibitory effect.

Next, we filtered CM from PRp cells to remove any factors that are larger than 3 kDa. The CM depleted of factors larger than 3 kDa retained its ability to block proliferation of $CD8^+$ T cells (Figure 6B). To rule out the possibility of protein fragments in the CM playing a role in inhibition of T cells, we treated PRp CM (that had been depleted of factors larger than 3 kDa) with Proteinase K to digest any remaining protein fragments. Surprisingly, Proteinase K addition was sufficient to rescue proliferation of $CD8^+$ T cells activated in PRp CM (Figure 6C). Motivated by these data, we reasoned that small peptides, which can be secreted by cells and have been shown to exert a variety of biological functions,[54-57] may impact $CD8^+$ T cell proliferation. In support of this possibility, treatment of PRp CM with dextrancoated charcoal (DCC), which can bind to and remove a diversity of small molecules, rescued the proliferation of $CD8^+$ T cells exposed to PRp CM (Figure 6D).

Given the likelihood of a small peptide modulating $CD8^+$ T cell proliferation, we sought to identify the peptide (or peptides) secreted by cells expressing Acod1. We therefore conducted mass spectrometry (MS) analysis on CM collected from different conditions. Since the factor would be more abundant in inhibitory CM, we sorted our results for hits where the relative abundance of the compound in PRp CM was at least 2-fold higher than PRs. We then looked for candidates that were higher in the inhibitory CM (PRp, PRp Scr) and lower in the permissive conditions (PRs, PRp Acod1 KO, PRp+DCC) (Figure S6B). Interestingly, we discovered a candidate (hereby termed MW518) that was elevated in PRp CM compared to PRs CM that is also decreased in PRp CM when Acod1 is lost or when the CM is treated with DCC (Figure 6E). To assess whether the production of this unknown

MW518 candidate was dependent on Acod1-mediated ITA production in cancer cells, we added ITA at increasing concentrations to PRp Acod1 KO cells. While ITA addition was, as expected, sufficient to increase the succinate:malate ratio in these cells (Figure S6D), we did not observe a significant change in the production of the MW518 candidate (Figure S6E). These data suggest that the production of this unknown candidate may be dependent on a function of Acod1 independent of ITA production.

We then used chemical formula prediction (TraceFinder v.1.8.63.0, Thermo Scientific) from accurate mass MS1 data considering C, H, O, N, and S atoms and isotopologue pattern matching to reveal nine chemical formulae possibilities within ±2 ppm MS1 mass error (Figure S6C). Since we hypothesized that this unknown is a peptide, we further ruled out eight of these matches that contained at least one S since there is no possible peptide sequences containing methionine or cysteine, the only amino acids with sulfur, that have the mass of interest. This remaining putative chemical formula was $C_{20}H_{35}O_{10}N_6$. Orthogonally, we searched the unknown *m/z* using the METLIN database (excluding compounds with chlorine and/or fluorine atoms), a tandem MS experimental database over 700,000 molecular standards.[58] This revealed two possibilities (both with the same chemical formula of $C_{20}H_{35}O_{10}N_6$ as was revealed by chemical formula prediction): the pentapeptide NGTID or ASNDL (we were not able to resolve the order of the amino acids in these peptide sequences). Using standard curves for the NGTID and ASNDL peptides, we were able to estimate that the MW518 pentapeptide was produced at a quantity of ~10–15 nM (Figure S6F). Since spectral libraries do not exist for pentapeptides, preventing MS2 spectral matching, we opted to use a functional validation of this putative compound identification. We subsequently synthesized each of these pentapeptide species and treated cells with escalating doses of each pentapeptide (informed by our calculation in Figure S6F) to assess their capacity to impact $CD8^+$ T cell proliferation. While NGTID treatment did not have a discernible impact on $CD8^+$ T cell proliferation (Figure 6F), treatment with ASNDL led to a concentration-dependent reduction in $CD8^+$ T cell proliferation (Figure 6G). Taken together, our data suggest that Acod1 expression in cancer cells can lead to the secretion of immunomodulatory pentapeptide species that can negatively regulate proliferation in $CD8^+$ T cells.

DISCUSSION

We discovered that cancer cells resistant to αPD-1 ICB have profound changes in mitochondrial metabolism that impact the immune microenvironment. More specifically, αPD-1-resistant cancer cells were discovered to have high levels of ITA owing to a significant elevation in Acod1. Engineering αPD-1-resistant cancer cells to be deficient in Acod1 restores the sensitivity of tumors arising from these cells to αPD-1 ICB monotherapy. Mechanistically, we found that αPD-1-resistant cancer cells secrete factors into the extracellular environment that negatively impact both activation and proliferation of $CD8^+$ T cells. Surprisingly, this effect on $CD8^+$ T cells is not due to the secretion of ITA. Instead, αPD-1-resistant cancer cells secrete small peptides that antagonize $CD8^+$ T cell proliferation.

Our data reveal an important role for Acod1 in cancer cells and in the regulation of anti-tumor immunity. Our data are congruent with a previous analysis of a cohort of patients with metastatic melanoma demonstrating that elevated *ACOD1* expression correlates with both diminished responsiveness to ICB therapy and poor clinical outcomes.[31] As mentioned previously, *Acod1* expression has largely been studied in the myeloid lineage (e.g., monocytes, macrophages). However, our findings add to a growing body of evidence suggesting that the activity of Acod1 can alter the TME in a fashion that alters ICB sensitivity.[46] In particular, we report here that Acod1 is expressed in both human and mouse cancerous epithelial cells. Similarly, our data add to the growing body of literature focused on understanding the immunomodulatory properties of ITA, including recent work that links ITA to the modulation of regulatory T cell differentiation[30] and to the regulation of $CD8^+$ T cells.[31] The latter study presents intriguing data suggesting that ITA secreted by myeloid-derived suppressor cells (MDSCs) can be taken up by $CD8^+$ T cells to negatively impact activation and proliferation. While we did not observe evidence of ITA-mediated changes in $CD8^+$ T cell activation or proliferation (see Figure 5), we focused our analysis on a much lower concentration that was based on our ITA measurements in CM from PRp cells (in the nM range). It is thus possible that MDSC-derived ITA exists in higher concentrations in the extracellular environment and could be somehow distinct from cancer-cell-derived ITA. Relatedly, immunomodulatory derivatives of ITA (e.g., citraconate and mesaconate) have recently been discovered.[59,60] While the mechanisms by which these derivatives are generated remain elusive, it is possible that there are important differences in ITA derivatization in distinct cell types that may impact its biological activities.

Our data suggest that the activity of Acod1 can cause cancer cells to secrete small immunomodulatory peptides that negatively impact $CD8^+$ T cell proliferation. More specifically, we identified a candidate peptide (consistent with the ASNDL sequence) in CM collected from cancer cells with elevated Acod1. While our data demonstrate that the production of this peptide is dependent on Acod1 levels in cancer cells and that addition of exogenous ASNDL can inhibit $CD8^+$ T cell proliferation, it remains possible that there are other small peptides with similar effects on $CD8^+$ T cells. Future studies aimed at systematically studying the configuration of immunomodulatory small peptides could be informative in leveraging these findings for clinical translation. Additionally, the mechanism by which Acod1 leads to the generation and secretion of peptides like ASNDL will require future study. Intriguingly, a recent study discovered that Acod1-mediated ITA can promote lysosomal biogenesis through a mechanism dependent on transcription factor EB.[61] It thus seems plausible that ITA-mediated changes in lysosomal activity could impact protein degradation in a fashion that produces immunomodulatory peptides like ASNDL.

Limitations of the study

Our findings suggest that loss of Acod1 in cancer cells sensitizes tumors to αPD-1 therapy, which is corroborated by clinical data in melanoma showing that patients with low *Acod1* gene scores have an increased response to αPD-1.[31,62] However, we did not have access to a dataset of human responders vs. non-responders to αPD-1 in prostate cancer, which would provide a more direct comparison to our findings. Additionally, matched clinical specimens of human patients could provide insight into the role of Acod1 in impacting the efficacy

of αPD-1. Moreover, we used genetic approaches to demonstrate the necessity of Acod1 in promoting immune evasion in Figures 3 and 4. To our knowledge, there does not yet exist a validated pharmacological inhibitor of Acod1 enzymatic activity, which would be helpful in both corroborating our findings and in future studies as well. Lastly, although we do identify a link between Acod1 and the generation of immunomodulatory pentapeptides, we have not yet delineated the mechanism by which these peptides are produced, nor do we understand the nature of their interactions with $CD8^+$ T cells. As such, additional studies investigating these questions will provide further context to the role Acod1 plays in immune evasion.

STAR★METHODS

RESOURCE AVAILABILITY

Lead contact—Further information and requests for resources and reagents should be directed to and will be fulfilled by the Lead Contact, Zachary T. Schafer (zschafe1@nd.edu).

Materials availability—Plasmids and/or cell lines generated in this study are available upon reasonable request. Unique reagents generated by this study are available after completion of an MTA. Please contact the lead contact.

Data and code availability

- All data reported in this paper will be shared by the lead contact upon request.
- This paper does not report original code.
- Any additional information required to reanalyze the data reported in this paper is available from the lead contact upon request.
- The metabolomics data are deposited on ProteomeXChange: PXD050289 (also provided in key resource table). The data will be publicly available as of the date of publication.

EXPERIMENTAL MODEL AND SUBJECT DETAILS

Mice—C57BL/6N mice were purchased from Envigo RMS LLC and maintained at the University of Notre Dame under approved protocols. Experiments were performed using male mice between 8 and 20 weeks of age. C57BL/6J mice were purchased from The Jackson Laboratory and maintained at VAI under approved protocols. Experiments with these mice were performed using female mice between 8 and 20 weeks of age.

Cell lines—MDA-MB-436, PC3, 293T and GCT were purchased from ATCC. DU145 cells were a kind gift from Jianneng Li (Notre Dame). PRs and PRp were developed from a spontaneous prostate tumor of *PB-Cre*$^+$ *Pten*$^{L/L}$ *Tp53* $^{L/L}$ *Smad4*$^{L/L}$ transgenic mice.[33] MDA-MB-436, 293T, PRs, and PRp were cultured in DMEM (Gibco). DU145 and PC3 were cultured in RPMI-1640 (Gibco). GCT cells were cultured in McCoy's 5A Medium (Gibco). All media were supplemented with 10% FBS (Invitrogen) and cells were cultured in the presence of 1% penicillin/streptomycin (HyClone). MDA-MB-436 and 293T cells are female. PC3, DU145, GCT, PRs, and PRp cells are male. All cell lines were cultured in a

humidified incubator at 37°C with 5% CO_2. All cells were tested routinely for mycoplasma-free status by PCR kit (Bulldog Bio, 25234).

Naive CD8$^+$ T cells—To isolate naive CD8$^+$ T cells, spleens from 8 week old C57BL/6N (Envigo) mice were harvested and single cell suspensions were generated by passing through a 70 μm filter (Falcon; 352350) then red blood cells were lysed with ACK lysis buffer (Gibco; A1049201) for 2 min on ice. Naive CD8$^+$ T cells were then purified from total lymphocytes by negative selection according to the manufacturer's instructions (Miltenyi Biotec; 130-096-543) and cultured in DMEM containing 10% FBS, 1% penicillin/streptomycin, and 2-ME (Gibco). For *in vitro* analysis, naive CD8$^+$ T cells were stimulated with αCD3 and αCD28 mAb-coated dynabeads (Thermo Fisher Scientific; 11452D).

METHOD DETAILS

Lentiviral transduction—Lentiviral constructs with gRNA targeting mouse Acod1 (5′-GGGCTTCCGATAGAGCTGTG-3′ and 5′-AACGTTGGTATTGAAGTACA-3′), or SCR gRNA (5′-GTGTAGTTCGACCATTCGTG-3′) in the puromycin-selectable pLV-hCas9 vector were purchased from VectorBuilder (Chicago, IL). HEK293T cells were transfected with target DNA along with the packaging vectors psPAX2 and pCMV-VSV-G using Lipofectamine 2000 (Invitrogen). Virus was collected 48h after transfection, filtered through a 0.45 μm filter (EMD Millipore), and used for transduction of PRp cells in the presence of 8 μg mL^{-1} polybrene. Stable polyclonal populations of cells were selected using 3 μg mL^{-1} puromycin (Invitrogen).

Mitochondrial measurements—Mitochondrial abundance was measured with MitoTracker Red CM-H_2XRos (Invitrogen, M7513). Cells were washed with PBS and stained with 100nM of MitoTracker in growth media for 30 min at 37°C. After incubation, cells were either counterstained with Hoechst 33342 (Invitrogen; H1399) and fixed with 4% PFA for 15 min for analysis by confocal fluorescence microscopy or washed with PBS and analyzed by flow cytometry. Confocal microscopy was conducted using a Nikon A1R-MP microscope (Nikon, Melville, NY). Maintenance of mitochondrial pool was assessed by the median fluorescence intensity (MFI) ratio of each cell line using the attached conditions as an internal control.

Immunoblotting—Attached and ECM-detached cells were washed once with ice-cold PBS and lysed in RIPA buffer (50 mM Tris (pH 8.0), 150 mM NaCl, 1% Nonidet P-40, 0.5% Sodium deoxycholate, 0.1% SDS) supplemented with 1 mg mL^{-1} aprotinin, 5 mg mL^{-1} leupeptin, 20 mg mL^{-1} phenylmethylsulfonyl fluoride (PMSF) and HALT phosphatase inhibitor mixture (Thermo Fisher Scientific). Lysates were collected after centrifugation for 15 min at 4°C at 14,000 r.p.m. and normalized by BCA assay (Pierce Biotechnology). Normalized lysates underwent SDS-PAGE and transfer/blotting were carried out as described previously.[63] The following primary antibodies were used for western blotting: β-actin (Sigma-Aldrich; A1978) (1:10000), Vinculin (Proteintech; 66305-1-Ig) (1:3000), mouse Irg1/Acod1 (Cell Signaling Technology (CST); 17805) (1:1000), human IRG1/ACOD1 (CST; 77510) (1:1000), Tim23 (BD Biosciences; 611222 (1:2000), Tom20 (CST; 42406) (1:1000), Sdhb (Proteintech; 10620-1-AP) (1:10000).

Secondary antibodies used were Alexa Fluor Plus 680 and 800 (Thermo Fisher Scientific; A32788, A32808) (1:10000) against mouse and rabbit, respectively, and bands were visualized with the LiCor Odyssey CLx (Licor).

Soft Agar assay—Cells were plated at $1x10^4$ cells per well in 1.5 mL of growth medium plus 0.4% low-melt agarose (Invitrogen) and layered onto a 3 mL bed of growth medium with 0.5% low-melt agarose. Cells were fed every other day with fresh growth medium. On day 7, growth medium was removed and viable colonies were stained using iodonitrotetrazolium violet (INT-violet) (Sigma-Aldrich). Colony number was determined using ImageJ (National Institutes of Health, Bethesda, MD, USA).

RNA isolation and quantitative real-time PCR—Total RNA was isolated with Zymo Quick RNA Miniprep kit (Zymo Research, R1054). RNA (1μg) was reverse transcribed into complementary DNA using an iScript Reverse Transcription Supermix kit (Bio-Rad, Hercules, CA, USA). The relative levels of gene transcripts compared with the control gene 18S were determined by quantitative real-time PCR using SYBR Green PCR Supermix (Bio-Rad) and specific primers on a 7,500 fast real-time PCR system (Applied Biosystems, Life Technologies, Waltham, MA, USA). Amplification was carried out at 95 °C for 12 min, followed by 40 cycles of 15 s at 95 °C, and 1 min at 60 °C. Error bars represent s.e.m., and p-values were calculated using a one-way ANOVA. The fold change in gene expression was calculated as $2^{-\Delta\Delta CT}$ and normalized to attached PRs cells. The primers used were as follows:

Acod1: F: GCAACATGATGCTCAAGTCTG and R: TGCTCCTCCGAATGATACCA.

18S: F: GGCGCCCCCTCGATGCTCTTAG and R: GCTCGGGCCTGCTTTGAACACTCT.

Metabolic tracing experiments—Cells were cultured in their respective media in detached (6 mg mL^{-1} poly-HEMA coated) plates for 20 h. Cells were then collected, washed with PBS, and replated in either uniformly labeled ^{13}C-Glucose (Cambridge Isotope Labs; CLM-1396) and unlabeled ^{12}C-Glutamine (Sigma-Aldrich; 49419), or unlabeled ^{12}C-Glucose (Sigma-Aldrich; G7021) and uniformly labeled ^{13}C-Glutamine (Cambridge Isotope Labs; CLM-1822) and incubated in a 37°C humidified incubator with 5% CO_2 for another 4 h. Cells were then centrifuged for 1 min at 900 RPM at 4°C to pellet the cells. Supernatant was collected and snap-frozen in liquid nitrogen. Cell pellets were washed briefly with ice-cold 0.9% NaCl, centrifuged to remove remaining media and snap-frozen in liquid nitrogen.

Metabolites were extracted with the Bligh-Dyer method.[64] The polar metabolite containing aqueous phase was dried and resuspended in 50 mL H_2O. For glucose and glutamine tracing and profiling experiments, LC-MS analysis was conducted on an Orbitrap ID-X (Thermo) as previously described.[65,66] Briefly, negative mode analytes were assessed using a Waters BEH Amide column (1.7 μm, 2.1 mm × 150 mm, #176001909, Waters, Eschborn, Germany). Mobile Phase A was 10mM ammonium acetate, 0.1% ammonium hydroxide, 0.1% medronic acid and mobile phase B was 90% ACN, 10mM ammonium acetate, 0.1% ammonium hydroxide, 0.1% medronic acid). The analytical gradient at a flow rate of 400

μL/min was: 0–1.0 min ramp from 100% B to 90% B, 1.0–12.5 min from 90% B to 75% B, 12.5–19 min from 75% B to 60% B, and 19–20 min hold at 60% B. Following every analytical separation, the column was re-equilibrated for 20 min as follows: 0–1 min hold at 65%B at 400 μL/min, 1–3 min hold at 65% B and ramp from 400 μL/min to 800 μL/min, 3–14 min hold at 65% B and 800 μL/min, 14–14.5 min ramp from 65% B to 100% B at 800 μL/min, 14.5–16 min hold at 100% B and increase flow from 800 μL/min to 1200 μL/min, 16–18.4 min hold at 100% B at 1200 μL/min, 18.4–19.5 min hold at 100% B and decrease flow from 1200 μL to 400 μL/min, 19.5–20 min hold at 100% B and 400 μL/min. The column temperature was maintained at 40°C Positive mode analytes were separated with a Waters T3 column (1.6 μm, 2.1 mm × 150 mm, #186008500, Waters). Mobile phase A was water with 0.1% formic acid and mobile Phase B: ACN with 0.1% formic acid. The analytical gradient at 300μL/min was 0–10 min ramp from 0%B to 30%B, 10–16 min ramp from 30%B to 100%B, and 16-20 min at 100%B. For both methods, column temperature was 40°C. MS source parameters were: spray voltage of 2500 V(negative mode)/3500 V(positive mode), sheath gas: 60 a.u., aux gas: 19 a.u., sweep gas: 1 a.u., ion transfer tube: 300°C, vaporizer: 300°C. MS. Experimental replicates were analyzed in MS1 only at a resolution of 120K (FWHM_ with a full scan range from 70 to 1000 m/z. ddMS2 was performed on pooled samples for compound identification as follows: MS1 resolution at 60K, MS2 resolution at 30K, intensity threshold at 2.0×10^4, and dynamic exclusion for 10s. MS2 fragmentation was completed first with HCD using stepped collision energies at 20, 35, and 50% and then CID in assisted mode at 15, 30, and 45% with an activation Q of 0.25.Data were analyzed using EL-Maven and Compound Discoverer (v 3.1, Thermo).

To confirm loss of ACOD1 activity in the Acod1 KO cells, $4x10^5$ PRp Scr or Acod1 KO cells/well were plated in 6-well poly-HEMA coated plates and stored in a 37°C humidified incubator with 5% CO_2 for 24 h. After 24 h, cells were then collected, washed with PBS, and replated in uniformly labeled ^{13}C-Glucose and placed back into the incubator for another 24 h. Cells and supernatant were then processed as previously stated and subjected to Bligh-Dyer metabolite extraction (above) to detect ^{13}C-labeled-ITA in either the intracellular cell pellet or the secretome. Data were collected on an Orbitrap Exploris 240 mass spectrometer (Thermo) using a tributylamine ion-paired reversed phase chromatography. The column was a ZORBAX Rapid Resolution HD (2.1 × 150 mm, 1.8 μm; 759700–902, Agilent). Mobile phase A was 3% methanol, and mobile phase B was 100% methanol. Both mobile phases contained 10 mM tributylamine (90780, SigmaAldrich, St Louis, MO, USA), 15 mM acetic acid and 2.5 μM medronic acid (5191–4506, Agilent Technologies, Santa Clara, CA, USA). The LC gradient was: 0–2.5 min 0% B, 2.5–7.5 min ramp to 20% B, 7.5–13 min ramp to 45% B, 13–20 min ramp to 99% B, 20–24 min hold at 99% B. Flow rate was 0.25 mL/min, and the column compartment was heated to 35°C. The column was then backflushed with 100% acetonitrile for 4 min (ramp from 0.25 to 0.8 mL/min in 1.5 min) and re-equilibrated with mobile phase A for 5 min at 0.4 mL/min. The H-ESI source was operated at spray voltage of −2500 V, sheath gas: 60 a.u., aux gas: 19 a.u., sweep gas: 1 a.u., ion transfer tube: 300°C, vaporizer: 250°C. Full scan MS1 data were collected from 70 to 800 m/z at mass resolution of 240,000 FWHM with RF lens at 35%, and standard automatic gain control (AGC). ddMS2 data were collected on pooled samples

using HCD fragmentation as described above. Data were analyzed in Compound Discoverer (v 3.3).

Itaconate quantification—$4x10^5$ PRs or PRp cells/well were plated in 6-well poly-HEMA coated plates in 4 mL of complete DMEM/well in triplicate and stored in a 37°C humidified incubator with 5% CO_2 for 48 h. Cells and supernatant were then processed as previously stated. A standard curve of neat itaconate (Sigma-Aldrich; I29204) was prepared using half-log dilutions from 316.23μM to 0.001μM, plus neat solvent as a zero blank. Equal volumes Samples and standards were extracted in 1mL of ice-cold acetonitrile:methanol:water (4:4:2 v/v). Data were collected using the tributylamine ion-paired reversed phase chromatography on the Orbitrap Exploris 240 as described above. Peak picking and integration was conducted in Skyline. Linear regression of standard curve peak areas were used to calculate ITA concentration in experimental samples.

Metabolic analysis of conditioned media—To screen CM for peptide and other small-molecule candidate effectors, compounds were extracted from CM using a modified Bligh-Dyer extraction (200μL of conditioned media added to 690μL of 1:1 chloroform:methanol and 110 μL of water). The aqueous layer was collected, dried, and resuspended in 100μL of water. To maximize compound coverage, 4uL of each sample were injected twice on an Orbitrap ID-X, one for ESI positive mode and one for ESI negative mode, on each of the BEH amide and T3 chromatographies described above. Full scan data were analyzed in Compound Discoverer (v3.3) to identify candidate features. Candidate features were interrogated using chemical formula prediction (Tracefinder) and MS2 spectral matching (mzCloud, NIST2020).

To estimate the concentration of the unknown MW518 ([M + H] = 519.2411 m/z; predicted chemical formula C20H24O10N6), we used synthetic isomeric peptides (ASNDL and NTGID, from Peptide 2.0) to prepare neat half-log step serial dilutions from 10μM to 1nM. These peptides closely elute with the unknown MW518 for approximation of local matrix effects and supports the putative identity of MW518 as a peptide. Media samples (prepared as described above) and standard curves for each peptide were analyzed by hydrophilic-interaction (HILIC) chromatography coupled to an Orbitrap ID-X mass spectrometry. Mobile phase A composition was LC/MS grade water (W6-4, Fisher) with a pH of 9.5 and mobile phase B composition was 90% LC/MS grade acetonitrile (A955, Fisher) with 10% LC/MS grade water at a pH of 8, and both mobile phases contained 0.1% ammonium hydroxide (A470, Fisher) and 10mM ammonium bicarbonate (533005, Sigma). LC separation was conducted with an Atlantis Premier BEH Z-HILIC column (1.7 μm, 2.1 mm × 150 mm, #186009980, Waters, Eschborn, Germanywith the following gradient: 0–1 min ramp from 0% A to 10% A, 1–10 min ramp from 10% A to 20% A, 10–14 min ramp from 20% A to 40% A. and 14–15 min held at 40% A. Column temperature was 40°C, analytical flow rate was kept at 0.4 mL/min, and sample injections were 4uL. For every injection, the analytical solvent gradient was followed by a 10 min wash gradient for column clean up and re-equilibration before the next sample injection. The wash gradient was as follows: 0–1 min ramp from 40% A to 80% A at 0.4 mL/min, 1–2 min held at 80% A and ramp from 0.4 mL/min to 0.6 mL/min, 2–4 min held at 80% A and 0.6 mL/min,

4–7.5 min ramp from 80% A to 0% A at 0.6 mL/min, 7.5–9 min held at 0% A and 0.6 mL/min, 9–9.5 min held at 0% A and ramp from 0.6 mL/min to 0.4 mL/min, and 9.5–10 min held at 0% A and 0.4 mL/min. Peptides and MW518 were detected by an Orbitrap ID-X using a tSIM scan (509.0248–529.0248 m/z range) in ESI-positive mode. Source and MS parameters were: source voltage 3500V, sheath gas 60, aux gas 19, sweep gas 1, ion transfer tube temperature 300°C, vaporizer temperature 250° C, and orbitrap resolution 120,000. Peak areas were determined in Skyline. The average response of NTGID and ASNDL peptides at each standard curve level was used to estimate MW518 concentration using linear regression.

Chemical reagents—The NF-κB inhibitor BAY1170-82 (Sigma-Aldrich; B5556) was used at 2.5 μM on ECM-detached PRp cells for 9 h in detachment. Cells were then collected and processed for immunoblotting or RNA extraction and qRT-PCR. The mitochondrial uncoupler CCCP (Sigma-Aldrich; C2759) was used at 20μM and added to PRp cells in detachment for the indicated time. Cells were collected and processed for immunoblotting as described above.

Exogenous ITA experiments—Itaconic acid (ITA) (Sigma-Aldrich; I29204) was freshly made before use in the media used for the assay. The pH of the ITA solutions were adjusted to 7.4 using NaOH, and then used at the given concentrations listed in the experiment.

Conditioned media—Conditioned Media (CM) was generated by plating $4x10^5$ cells/well in a poly-HEMA coated 6-well plate in 4 mL total volume of respective media. After 48 h of incubation, we harvested the supernatant, centrifuged at 10,000g for 15 min at 24°C, collected the supernatant, aliquoted, snap-froze in liquid nitrogen, and stored at −80°C until ready to use in experiments. For all *in vitro* assays involving naive $CD8^+$ T cells, the CM was diluted 1:1 with fresh medium.

EdU incorporation assay—EdU (5-ethynyl-2′-deoxyuridine) was diluted in media and added to cells for 4 h at 37°C in a humidified incubator with 5% CO_2. After incubation, T cells were washed in 1x PBS, replated into a 96-well plate, and fixed using 4% PFA for 15 min. The Click-iT EdU kit (Thermo Fisher; C10340) AF^+647 was used according to the manufacturer's instructions. Cells were counterstained with 4′,6-diamidino-2-phenylindole (DAPI) (Invitrogen; D3571) (1:2000) for 10 min and then imaged on a Zeiss inverted light microscope (Carl Zeiss, Axio Observer). Images were processed in ImageJ to get %EdU+, which was scored as (cells EdU+/cells DAPI+)*100.

***In vitro* T cell activation assays—**Naive $CD8^+$ T cells were purified from the spleens of female C57BL6/J mice (Jackson Laboratories) by negative selection (StemCell Technologies; 19858A). To evaluate cell proliferation by Violet Proliferation Dye 450 (VPD450) dilution, cells were stained with VPD450 according to the manufacturer's instructions (BD Biosciences; 562158). $1.5x10^5$ naive $CD8^+$ T cells were seeded per well of a 96-well plate coated with αCD3ε (clone 145-2C11; 2 μg/mL) and αCD28 (clone 37.51; 1 μg mL^{-1}) antibodies (eBioscience). Cells were seeded in 100 μL of Iscove's Modified Dulbecco's Medium (IMDM) supplemented with 10% Nu-Serum IV culture supplement (Corning), 1% penicillin/streptomycin, and 50 μM 2-ME. For assays involving CM, 2-ME

was added to the CM at a final concentration of 50 μM, and then 100 μL of CM was added per well. For assays involving ITA, ITAwasdissolvedin IMDM and the pH adjusted to 7.4 prior to adding it to the cells at the indicated final concentrations. Cells were incubated at 37°C in a humidified incubator with 5% CO_2 for 72 h. To assess cytokine production, cells were treated with phorbol 12-myristate 13-acetate (PMA; 50 ng mL^{-1}) and ionomycin (500 ng mL^{-1}) for 4 h at 37°C, with GolgiStop (BD Biosciences; 1:1500 dilution) added for the last 2 h of stimulation prior staining for flow cytometry. After PMA/ionomycin stimulation, the cells were stained with cell surface marker antibodies and a cell viability dye for 1 h at 4°C, fixed and permeabilized using the FoxP3/Transcription Factor Staining Buffer Set (eBioscience, 51-2092KZ) for 1 h at 4°C, and then stained with intracellular marker antibodies for 1 h at 4°C. The following antibodies were used for flow cytometry: CD8α-BUV395 (BD Biosciences; 563786), CD4-BV605 (BioLegend; 100548), CD25-Alexa Fluor 488 (eBioscience; 53-0251-82), CD44-BUV805 (BD Biosciences; 741921) IFN-γ-APC (eBioscience; 17-7311-82), Granzyme B-PE/Dazzle 594 (BioLegend; 372216). Cell viability was assessed by using Fixable Viability Dye eFluor 780 (eBioscience, 65-0865-14) according to the manufacturer's protocol. Analytical flow cytometry was performed using a Cytek Aurora cytometer and data analysis performed using FlowJo (Tree Star) software.

Heat-inactivation treatment of conditioned media—To heat-inactivate the polypeptide component of the supernatant, collected CM were boiled for 5 min at 100°C. After cooling, boiled CM was used 1:1 with fresh media for *in vitro* T cell assays as previously stated.

Dextran-coated charcoal (DCC)—To remove small molecules, the CM were treated with DCC, which removes small molecules (e.g., nucleotides, lipids, peptides) by binding them on the surface. 12 mg of DCC per 500 μL of CM was added and incubated for 20 min at 25°C, followed by centrifugation at 10,000g for 30 min. After centrifugation, the supernatant that was cleared by the DCC was collected, snap-frozen in liquid nitrogen, and stored in −80°C until use.

Fractionation of conditioned media and Proteinase K treatment—Culture supernatants were fractionated using Amicon ultra-centrifugal filters (Millipore Sigma; UFC900324) with 3 kDa cut-off. Supernatants were added to the 3 kDa filter and centrifuged at 12,000g for 30 min at 4°C. The filtered supernatant was collected and either stored as previously described or further treated with Proteinase K. For Proteinase K, 2 mg mL^{-1} of Proteinase K (Sigma-Aldrich) was added to filtered CM and incubated for 40 min at 37°C. Proteinase K-treated CM was added to a new 3 kDa filter and centrifuged at 12,000g for 30 min at 4°C to remove the Proteinase K.

Mouse tumor experiment—All animal work performed in this study was approved (19-10-5588) by the Institutional Animal Care and Use Committee (IACUC) at the University of Notre Dame. Male C57BL/6N mice, 6 weeks old, were acquired from Envigo Laboratories. $5x10^5$ tumor cells were injected subcutaneously into the flank of 8-week-old mice. Once tumors reached ≥50 mm^3, mice were i.p.-injected with 10 mg/kg of αPD-1 mAb (clone RMP1-14); the mAb treatment was repeated every third day. For control groups,

an isotype control for the αPD-1 mAb (Rat IgG2a, κ) (clone RTK2758) was injected on the same schedule. Tumor sizes were measured every third day using a digimatic caliper (Louisware) and tumor volume was calculated using the formula [(length x width^2)/2].

Fluorescent immunohistochemistry (IHC)—For tumor IHC, tumor samples were collected from each treatment group and fixed in 10% neutral buffered formalin (NBF). Paraffin-embedded sections (4 μm) were deparaffinized in xylene, then rehydrated through graded alcohol and washed briefly in ddH_2O. Antigen retrieval was performed by boiling sections in SignalStain Citrate Unmasking (CST) for 10 min in microwave. Sections were left to room temperature and washed briefly in PBS. Sections were blocked in 5% goat serum and 0.3% Triton X-100 diluted in PBS (pH 7.4) for 1 h at room temperature then washed in PBS. Subsequently, sections were incubated at 4°C overnight in primary antibody for Granzyme B (GzmB) (1:500) (CST; 98941S), rinsed with fresh PBS, and incubated with secondary antibody Alexa Fluor 647 goat anti-rabbit immunoglobulin (IgG) (1:500) (Thermo Fisher; A-21245) at room temperature for 1 h protected from light, then washed briefly with PBS. Terminal deoxynucleotidyl transferase dUTP nick end labeling (TUNEL) was performed using the *In Situ* Cell Death Detection Kit (Roche; 12156792910) according to the manufacturer's instructions protected from light. Sections were then washed with PBS and counterstained with DAPI (1:2000) for 10 min at room temperature protected from light. Last, sections were mounted in ProLong Gold antifade and imaged on a Leica SP8 laser scanning confocal microscope. For TUNEL+ quantification, the average cell number with standard deviation (SD) was determined from six random high-powered fields-of-view (FOV). Granzyme B intensity was normalized by calculating the fluorescence intensity of Gzmb in each image/DAPI intensity for cell number.

Tumor immunophenotyping—Tumors were minced and digested in complete DMEM with 10% FBS and 1 mg/mL collagenase IV (Invitrogen; 17104019) at 37°C for 1 h, followed by passing through 40 μm strainers. Erythrocytes were lysed with ACK lysis buffer. Cells were treated with mouse Fc-block αCD16/32 (BioLegend; 101302) for 10 min, and stained with primary fluorophore-conjugated antibodies for 30 min. CD45-FITC (35–0451), CD4-APC (20–0041), and CD8-PE (50–1886) were used in the antibody cocktail (Tonbo Biosciences). Cells were washed, resuspended in Live/Dead Aqua 405 nm (Invitrogen) for 15 min, washed again, and then analyzed on a BD LSRFortessa X-20 cytometer.

Peptide assays—NGTID and ASNDL peptides were synthesized to >95% purity by Peptide 2.0 (Chantilly, VA). Peptides stocks were resuspended in 50% MeOH and 50% ultra-pure H_2O, aliquoted, and stored at −80°C. Each peptide was used fresh in the indicated assays and diluted to the working concentrations shown in their respective media. For most assays, peptides were used at 0.1, 10, and 1000 nM, unless otherwise indicated.

QUANTIFICATION AND STATISTICAL ANALYSIS

Statistical analyses were performed using GraphPad Prism v9.0. Unless otherwise mentioned, all data are presented as mean ± SEM (standard error of the mean). Sample

sizes, error bars, p values, and statistical methods are denoted in figure legends. Statistical significance was defined as $p < 0.05$.

Supplementary Material

Refer to Web version on PubMed Central for supplementary material.

ACKNOWLEDGMENTS

We thank Veronica Schafer and all current/past Schafer lab members for helpful comments and/or valuable discussion. We thank Jianneng Li (Notre Dame) for the DU-145 cells, Sara Cole (Notre Dame Integrated Imaging Facility) for assistance with confocal microscopy, and the staff at the Freimann Life Science Center for assistance with animal care. Z.T.S. is supported by the National Institutes of Health/National Cancer Institute (R01CA262439), the Coleman Foundation, the Malanga Family Excellence Fund for Cancer Research at Notre Dame, the College of Science at Notre Dame, the Department of Biological Sciences at Notre Dame, and funds from Mr. Nick L. Petroni. X.L. (R01CA248033, R01CA280097) and S.M. (5F99CA274694) are also supported by the National Institutes of Health/National Cancer Institute. R.G.J. is supported by the Paul G. Allen Frontiers Group Distinguished Investigator Program, the National Institutes of Health/National Institute of Allergy and Infectious Diseases (R01AI165722), and VAI. The graphical abstract, the schematic in Figure 3, and Figure S1 were created with BioRender.com.

REFERENCES

1. Huang AC, and Zappasodi R (2022). A decade of checkpoint blockade immunotherapy in melanoma: understanding the molecular basis for immune sensitivity and resistance. Nat. Immunol 23, 660–670. 10.1038/s41590-022-01141-1. [PubMed: 35241833]
2. Pardoll DM (2012). The blockade of immune checkpoints in cancer immunotherapy. Nat. Rev. Cancer 12, 252–264. 10.1038/nrc3239. [PubMed: 22437870]
3. Khalil DN, Smith EL, Brentjens RJ, and Wolchok JD (2016). The future of cancer treatment: immunomodulation, CARs and combination immunotherapy. Nat. Rev. Clin. Oncol 13, 273–290. 10.1038/nrclinonc.2016.25. [PubMed: 26977780]
4. Alsaab HO, Sau S, Alzhrani R, Tatiparti K, Bhise K, Kashaw SK, and Iyer AK (2017). PD-1 and PD-L1 Checkpoint Signaling Inhibition for Cancer Immunotherapy: Mechanism, Combinations, and Clinical Outcome. Front. Pharmacol 8, 561. 10.3389/fphar.2017.00561. [PubMed: 28878676]
5. Larkin J, Chiarion-Sileni V, Gonzalez R, Grob JJ, Cowey CL, Lao CD, Schadendorf D, Dummer R, Smylie M, Rutkowski P, et al. (2015). Combined Nivolumab and Ipilimumab or Monotherapy in Untreated Melanoma. N. Engl. J. Med 373, 23–34. 10.1056/NEJMoa1504030. [PubMed: 26027431]
6. Borghaei H, Paz-Ares L, Horn L, Spigel DR, Steins M, Ready NE, Chow LQ, Vokes EE, Felip E, Holgado E, et al. (2015). Nivolumab versus Docetaxel in Advanced Nonsquamous Non–Small-Cell Lung Cancer. N. Engl. J. Med 373, 1627–1639. 10.1056/NEJMoa1507643. [PubMed: 26412456]
7. Garon EB, Rizvi NA, Hui R, Leighl N, Balmanoukian AS, Eder JP, Patnaik A, Aggarwal C, Gubens M, Horn L, et al. (2015). Pembrolizumab for the Treatment of Non-Small-Cell Lung Cancer. N. Engl. J. Med 372, 2018–2028. 10.1056/NEJMoa1501824. [PubMed: 25891174]
8. Morad G, Helmink BA, Sharma P, and Wargo JA (2021). Hallmarks of response, resistance, and toxicity to immune checkpoint blockade. Cell 184, 5309–5337. 10.1016/j.cell.2021.09.020. [PubMed: 34624224]
9. Fares CM, Van Allen EM, Drake CG, Allison JP, and Hu-Lieskovan S (2019). Mechanisms of Resistance to Immune Checkpoint Blockade: Why Does Checkpoint Inhibitor Immunotherapy Not Work for All Patients? Am. Soc. Clin. Oncol. Educ. Book 39, 147–164. 10.1200/edbk_240837. [PubMed: 31099674]
10. Topalian SL, Hodi FS, Brahmer JR, Gettinger SN, Smith DC, McDermott DF, Powderly JD, Carvajal RD, Sosman JA, Atkins MB, et al. (2012). Safety, Activity, and Immune Correlates of Anti–PD-1 Antibody in Cancer. N. Engl. J. Med 366, 2443–2454. 10.1056/NEJMoa1200690. [PubMed: 22658127]

11. Brahmer JR, Drake CG, Wollner I, Powderly JD, Picus J, Sharfman WH, Stankevich E, Pons A, Salay TM, McMiller TL, et al. (2023). Phase I Study of Single-Agent Anti-Programmed Death-1 (MDX-1106) in Refractory Solid Tumors: Safety, Clinical Activity, Pharmacodynamics, and Immunologic Correlates. J. Clin. Oncol 41, 715–723. 10.1200/jco.22.02270. [PubMed: 36706735]
12. Martinez-Usatorre A, Kadioglu E, Boivin G, Cianciaruso C, Guichard A, Torchia B, Zangger N, Nassiri S, Keklikoglou I, Schmittnaegel M, et al. (2021). Overcoming microenvironmental resistance to PD-1 blockade in genetically engineered lung cancer models. Sci. Transl. Med 13, eabd1616. 10.1126/scitranslmed.abd1616. [PubMed: 34380768]
13. DePeaux K, and Delgoffe GM (2021). Metabolic barriers to cancer immunotherapy. Nat. Rev. Immunol 21, 785–797. 10.1038/s41577-021-00541-y. [PubMed: 33927375]
14. Wang H, Rong X, Zhao G, Zhou Y, Xiao Y, Ma D, Jin X, Wu Y, Yan Y, Yang H, et al. (2022). The microbial metabolite trimethylamine N-oxide promotes antitumor immunity in triple-negative breast cancer. Cell Metabol. 34, 581–594.e8. 10.1016/j.cmet.2022.02.010.
15. Bender MJ, McPherson AC, Phelps CM, Pandey SP, Laughlin CR, Shapira JH, Medina Sanchez L, Rana M, Richie TG, Mims TS, et al. (2023). Dietary tryptophan metabolite released by intratumoral Lactobacillus reuteri facilitates immune checkpoint inhibitor treatment. Cell 186, 1846–1862.e26. 10.1016/j.cell.2023.03.011. [PubMed: 37028428]
16. Hezaveh K, Shinde RS, Klötgen A, Halaby MJ, Lamorte S, Ciudad MT, Quevedo R, Neufeld L, Liu ZQ, Jin R, et al. (2022). Tryptophan-derived microbial metabolites activate the aryl hydrocarbon receptor in tumor-associated macrophages to suppress anti-tumor immunity. Immunity 55, 324–340.e8. 10.1016/j.immuni.2022.01.006. [PubMed: 35139353]
17. Leone RD, and Emens LA (2018). Targeting adenosine for cancer immunotherapy. J. Immunother. Cancer 6, 57. 10.1186/s40425-018-0360-8. [PubMed: 29914571]
18. Michelucci A, Cordes T, Ghelfi J, Pailot A, Reiling N, Goldmann O, Binz T, Wegner A, Tallam A, Rausell A, et al. (2013). Immune-responsive gene 1 protein links metabolism to immunity by catalyzing itaconic acid production. Proc. Natl. Acad. Sci. USA 110, 7820–7825. 10.1073/pnas.1218599110. [PubMed: 23610393]
19. O'Neill LAJ, and Artyomov MN (2019). Itaconate: the poster child of metabolic reprogramming in macrophage function. Nat. Rev. Immunol 19, 273–281. 10.1038/s41577-019-0128-5. [PubMed: 30705422]
20. Runtsch MC, Angiari S, Hooftman A, Wadhwa R, Zhang Y, Zheng Y, Spina JS, Ruzek MC, Argiriadi MA, McGettrick AF, et al. (2022). Itaconate and itaconate derivatives target JAK1 to suppress alternative activation of macrophages. Cell Metabol. 34, 487–501.e8. 10.1016/j.cmet.2022.02.002.
21. Mills EL, Ryan DG, Prag HA, Dikovskaya D, Menon D, Zaslona Z, Jedrychowski MP, Costa ASH, Higgins M, Hams E, et al. (2018). Itaconate is an anti-inflammatory metabolite that activates Nrf2 viaalkylation of KEAP1. Nature 556, 113–117. 10.1038/nature25986. [PubMed: 29590092]
22. Swain A, Bambouskova M, Kim H, Andhey PS, Duncan D, Auclair K, Chubukov V, Simons DM, Roddy TP, Stewart KM, and Artyomov MN (2020). Comparative evaluation of itaconate and its derivatives reveals divergent inflammasome and type I interferon regulation in macrophages. Nat. Metab 2, 594–602. 10.1038/s42255-020-0210-0. [PubMed: 32694786]
23. Lampropoulou V, Sergushichev A, Bambouskova M, Nair S, Vincent EE, Loginicheva E, Cervantes-Barragan L, Ma X, Huang SCC, Griss T, et al. (2016). Itaconate Links Inhibition of Succinate Dehydrogenase with Macrophage Metabolic Remodeling and Regulation of Inflammation. Cell Metabol. 24, 158–166. 10.1016/j.cmet.2016.06.004.
24. Bambouskova M, Potuckova L, Paulenda T, Kerndl M, Mogilenko DA, Lizotte K, Swain A, Hayes S, Sheldon RD, Kim H, et al. (2021). Itaconate confers tolerance to late NLRP3 inflammasome activation. Cell Rep. 34, 108756. 10.1016/j.celrep.2021.108756. [PubMed: 33691097]
25. Strelko CL, Lu W, Dufort FJ, Seyfried TN, Chiles TC, Rabinowitz JD, and Roberts MF (2011). Itaconic acid is a mammalian metabolite induced during macrophage activation. J. Am. Chem. Soc 733, 16386–16389. 10.1021/ja2070889.
26. Wu R, Chen F, Wang N, Tang D, and Kang R (2020). ACOD1 in immunometabolism and disease. Cell. Mol. Immunol 17, 822–833. 10.1038/s41423-020-0489-5. [PubMed: 32601305]

27. Wu R, Kang R, and Tang D (2022). Mitochondrial ACOD1/IRG1 in infection and sterile inflammation. J. Intensive Med 2, 78–88. 10.1016/j.jointm.2022.01.001. [PubMed: 36789185]
28. Tomlinson KL, Riquelme SA, Baskota SU, Drikic M, Monk IR, Stinear TP, Lewis IA, and Prince AS (2023). Staphylococcus aureus stimulates neutrophil itaconate production that suppresses the oxidative burst. Cell Rep. 42, 112064. 10.1016/j.cel-rep.2023.112064. [PubMed: 36724077]
29. Zhao Y, Liu Z, Liu G, Zhang Y, Liu S, Gan D, Chang W, Peng X, Sung ES, Gilbert K, et al. (2023). Neutrophils resist ferroptosis and promote breast cancer metastasis through aconitate decarboxylase 1. Cell Metabol. 35, 1688–1703.e10. 10.1016/j.cmet.2023.09.004.
30. Aso K, Kono M, Kanda M, Kudo Y, Sakiyama K, Hisada R, Karino K, Ueda Y, Nakazawa D, Fujieda Y, et al. (2023). Itaconate ameliorates autoimmunity by modulating T cell imbalancevia metabolic and epigenetic reprogramming. Nat. Commun 14, 984. 10.1038/s41467-023-36594-x. [PubMed: 36849508]
31. Zhao H, Teng D, Yang L, Xu X, Chen J, Jiang T, Feng AY, Zhang Y, Frederick DT, Gu L, et al. (2022). Myeloid-derived itaconate suppresses cytotoxic CD8+ T cells and promotes tumour growth. Nat. Metab 4, 1660–1673. 10.1038/s42255-022-00676-9. [PubMed: 36376563]
32. Zeng YR, Song JB, Wang D, Huang ZX, Zhang C, Sun YP, Shu G, Xiong Y, Guan KL, Ye D, and Wang P (2023). The immunometabolite itaconate stimulates OXGR1 to promote mucociliary clearance during the pulmonary innate immune response. J. Clin. Invest 133, e160463. 10.1172/jci160463. [PubMed: 36919698]
33. Lu X, Horner JW, Paul E, Shang X, Troncoso P, Deng P, Jiang S, Chang Q, Spring DJ, Sharma P, et al. (2017). Effective combinatorial immunotherapy for castration-resistant prostate cancer. Nature 543, 728–732. 10.1038/nature21676. [PubMed: 28321130]
34. Murphy S, Rahmy S, Gan D, Zhu Y, Manyak M, Li J, Lu X, and Lu X (2023). Overcome Prostate Cancer Resistance to Immune Checkpoint Therapy with Ketogenic Diet-Induced Epigenetic Reprogramming. Preprint at bioRxiv. 10.1101/2023.08.07.552383.
35. Hawk MA, Gorsuch CL, Fagan P, Lee C, Kim SE, Hamann JC, Mason JA, Weigel KJ, Tsegaye MA, Shen L, et al. (2018). RIPK1-mediated induction of mitophagy compromises the viability of extracellular-matrix-detached cells. Nat. Cell Biol 20, 272–284. 10.1038/s41556-018-0034-2. [PubMed: 29459781]
36. Hawk MA, and Schafer ZT (2018). RIPK1-dependent mitophagy: A novel mechanism to eliminate cells detached from the extracellular matrix. Mol. Cell. Oncol 5, e1465015. 10.1080/23723556.2018.1465015. [PubMed: 30250916]
37. Schofield JH, and Schafer ZT (2021). Mitochondrial Reactive Oxygen Species and Mitophagy: A Complex and Nuanced Relationship. Antioxidants Redox Signal. 34, 517–530. 10.1089/ars.2020.8058.
38. Buchheit CL, Weigel KJ, and Schafer ZT (2014). Cancer cell survival during detachment from the ECM: multiple barriers to tumour progression. Nat. Rev. Cancer 14, 632–641. 10.1038/nrc3789. [PubMed: 25098270]
39. Mason JA, Hagel KR, Hawk MA, and Schafer ZT (2017). Metabolism during ECM Detachment: Achilles Heel of Cancer Cells? Trends Cancer 3, 475–481. 10.1016/j.trecan.2017.04.009. [PubMed: 28718402]
40. Faubert B, Solmonson A, and DeBerardinis RJ (2020). Metabolic reprogramming and cancer progression. Science 368, eaaw5473. 10.1126/science.aaw5473. [PubMed: 32273439]
41. Daniels BP, Kofman SB, Smith JR, Norris GT, Snyder AG, Kolb JP, Gao X, Locasale JW, Martinez J, Gale M Jr., et al. (2019). The Nucleotide Sensor ZBP1 and Kinase RIPK3 Induce the Enzyme IRG1 to Promote an Antiviral Metabolic State in Neurons. Immunity 50, 64–76.e4, e64. 10.1016/j.immuni.2018.11.017. [PubMed: 30635240]
42. Preusse M, Tantawy MA, Klawonn F, Schughart K, and Pessler F (2013). Infection- and procedure-dependent effects on pulmonary gene expression in the early phase of influenza A virus infection in mice. BMC Microbiol. 13, 293. 10.1186/1471-2180-13-293. [PubMed: 24341411]
43. Ren K, Lv Y, Zhuo Y, Chen C, Shi H, Guo L, Yang G, Hou Y, Tan RX, and Li E (2016). Suppression of IRG-1 Reduces Inflammatory Cell Infiltration and Lung Injury in Respiratory Syncytial Virus Infection by Reducing Production of Reactive Oxygen Species. J. Virol 90, 7313–7322. 10.1128/jvi.00563-16. [PubMed: 27252532]

44. Degrandi D, Hoffmann R, Beuter-Gunia C, and Pfeffer K (2009). The proinflammatory cytokine-induced IRG1 protein associates with mitochondria. J. Interferon Cytokine Res 29, 55–67. 10.1089/jir.2008.0013. [PubMed: 19014335]
45. Chen N, and Debnath J (2013). IκB kinase complex (IKK) triggers detachment-induced autophagy in mammary epithelial cells independently of the PI3K-AKT-MTORC1 pathway. Autophagy 9, 1214–1227. 10.4161/auto.24870. [PubMed: 23778976]
46. Chen YJ, Li GN, Li XJ, Wei LX, Fu MJ, Cheng ZL, Yang Z, Zhu GQ, Wang XD, Zhang C, et al. (2023). Targeting IRG1 reverses the immunosuppressive function of tumor-associated macrophages and enhances cancer immunotherapy. Sci. Adv 9, eadg0654. 10.1126/sciadv.adg0654. [PubMed: 37115931]
47. Tumeh PC, Harview CL, Yearley JH, Shintaku IP, Taylor EJM, Robert L, Chmielowski B, Spasic M, Henry G, Ciobanu V, et al. (2014). PD-1 blockade induces responses by inhibiting adaptive immune resistance. Nature 515, 568–571. 10.1038/nature13954. [PubMed: 25428505]
48. Nagata S. (1997). Apoptosis by Death Factor. Cell 88, 355–365. 10.1016/S0092-8674(00)81874-7. [PubMed: 9039262]
49. Darmon AJ, Nicholson DW, and Bleackley RC (1995). Activation of the apoptotic protease CPP32 by cytotoxic T-cell-derived granzyme B. Nature 377, 446–448. 10.1038/377446a0. [PubMed: 7566124]
50. Kumar A, Chamoto K, Chowdhury PS, and Honjo T (2020). Tumors attenuating the mitochondrial activity in T cells escape from PD-1 blockade therapy. Elife 9, e52330. 10.7554/eLife.52330. [PubMed: 32122466]
51. Meiser J, Kraemer L, Jaeger C, Madry H, Link A, Lepper PM, Hiller K, and Schneider JG (2018). Itaconic acid indicates cellular but not systemic immune system activation. Oncotarget 9, 32098–32107. 10.18632/oncotarget.25956. [PubMed: 30181801]
52. Cordes T, and Metallo CM (2021). Itaconate Alters Succinate and Coenzyme A Metabolism via Inhibition of Mitochondrial Complex II and Methylmalonyl-CoA Mutase. Metabolites 11, 117. 10.3390/metabo11020117. [PubMed: 33670656]
53. Nastasi C, Willerlev-Olsen A, Dalhoff K, Ford SL, Gadsbøll ASØ, Buus TB, Gluud M, Danielsen M, Litman T, Bonefeld CM, et al. (2021). Inhibition of succinate dehydrogenase activity impairs human T cell activation and function. Sci. Rep 11, 1458. 10.1038/s41598-020-80933-7. [PubMed: 33446766]
54. Apostolopoulos V, Bojarska J, Chai TT, Elnagdy S, Kaczmarek K, Matsoukas J, New R, Parang K, Lopez OP, Parhiz H, et al. (2021). A Global Review on Short Peptides: Frontiers and Perspectives. Molecules 26. 10.3390/molecules26020430.
55. Parvy JP, Yu Y, Dostalova A, Kondo S, Kurjan A, Bulet P, Lemaître B, Vidal M, and Cordero JB (2019). The antimicrobial peptide defensin cooperates with tumour necrosis factor to drive tumour cell death in Drosophila. Elife 8, e45061. 10.7554/eLife.45061. [PubMed: 31358113]
56. Miller B, Kim SJ, Kumagai H, Yen K, and Cohen P (2022). Mitochondria-derived peptides in aging and healthspan. J. Clin. Invest 132, e158449. 10.1172/jci158449. [PubMed: 35499074]
57. Welsh JB, Sapinoso LM, Kern SG, Brown DA, Liu T, Bauskin AR, Ward RL, Hawkins NJ, Quinn DI, Russell PJ, et al. (2003). Large-scale delineation of secreted protein biomarkers overexpressed in cancer tissue and serum. Proc. Natl. Acad. Sci. USA 100, 3410–3415. 10.1073/pnas.0530278100. [PubMed: 12624183]
58. Montenegro-Burke JR, Guijas C, and Siuzdak G (2020). METLIN: A Tandem Mass Spectral Library of Standards. Methods Mol. Biol 2104, 149–163. 10.1007/978-1-0716-0239-3_9. [PubMed: 31953817]
59. Chen F, Elgaher WAM, Winterhoff M, Büssow K, Waqas FH, Graner E, Pires-Afonso Y, Casares Perez L, de laVega L, Sahini N, et al. (2022). Citraconate inhibits ACOD1 (IRG1) catalysis, reduces interferon responses and oxidative stress, and modulates inflammation and cell metabolism. Nat. Metab 4, 534–546. 10.1038/s42255-022-00577-x. [PubMed: 35655026]
60. He W, Henne A, Lauterbach M, Geißmar E, Nikolka F, Kho C, Heinz A, Dostert C, Grusdat M, Cordes T, et al. (2022). Mesaconate is synthesized from itaconate and exerts immunomodulatory effects in macrophages. Nat. Metab 4, 524–533. 10.1038/s42255-022-00565-1. [PubMed: 35655024]

61. Zhang Z, Chen C, Yang F, Zeng YX, Sun P, Liu P, and Li X (2022). Itaconate is a lysosomal inducer that promotes antibacterial innate immunity. Mol. Cell 82, 2844–2857.e10. 10.1016/j.molcel.2022.05.009. [PubMed: 35662396]

62. Liu D, Schilling B, Liu D, Sucker A, Livingstone E, Jerby-Arnon L, Zimmer L, Gutzmer R, Satzger I, Loquai C, et al. (2019). Integrative molecular and clinical modeling of clinical outcomes to PD1 blockade in patients with metastatic melanoma. Nat. Med 25, 1916–1927. 10.1038/s41591-019-0654-5. [PubMed: 31792460]

63. Mason JA, Davison-Versagli CA, Leliaert AK, Pape DJ, McCallister C, Zuo J, Durbin SM, Buchheit CL, Zhang S, and Schafer ZT (2016). Oncogenic Ras differentially regulates metabolism and anoikis in extracellular matrix-detached cells. Cell Death Differ. 23, 1271–1282. 10.1038/cdd.2016.15. [PubMed: 26915296]

64. Bligh EG, and Dyer WJ (1959). A rapid method of total lipid extraction and purification. Can. J. Biochem. Physiol 37, 911–917. 10.1139/o59-099. [PubMed: 13671378]

65. Kaymak I, Luda KM, Duimstra LR, Ma EH, Longo J, Dahabieh MS, Faubert B, Oswald BM, Watson MJ, Kitchen-Goosen SM, et al. (2022). Carbon source availability drives nutrient utilization in CD8(+) T cells. Cell Metabol. 34, 1298–1311.e6. 10.1016/j.cmet.2022.07.012.

66. Ma EH, Verway MJ, Johnson RM, Roy DG, Steadman M, Hayes S, Williams KS, Sheldon RD, Samborska B, Kosinski PA, et al. (2019). Metabolic Profiling Using Stable Isotope Tracing Reveals Distinct Patterns of Glucose Utilization by Physiologically Activated CD8(+) T Cells. Immunity 51, 856–870.e5. 10.1016/j.immuni.2019.09.003. [PubMed: 31747582]

Highlights

- Cancerous epithelial cells can express *Acod1* and produce itaconate
- Acod1 loss in αPD-1-resistant tumors resensitizes them to therapy
- Acod1^{hi} cells inhibit naive CD8^{+} T cell activation independent of itaconate
- Acod1^{hi} cells suppress T cells by secreting inhibitory peptides

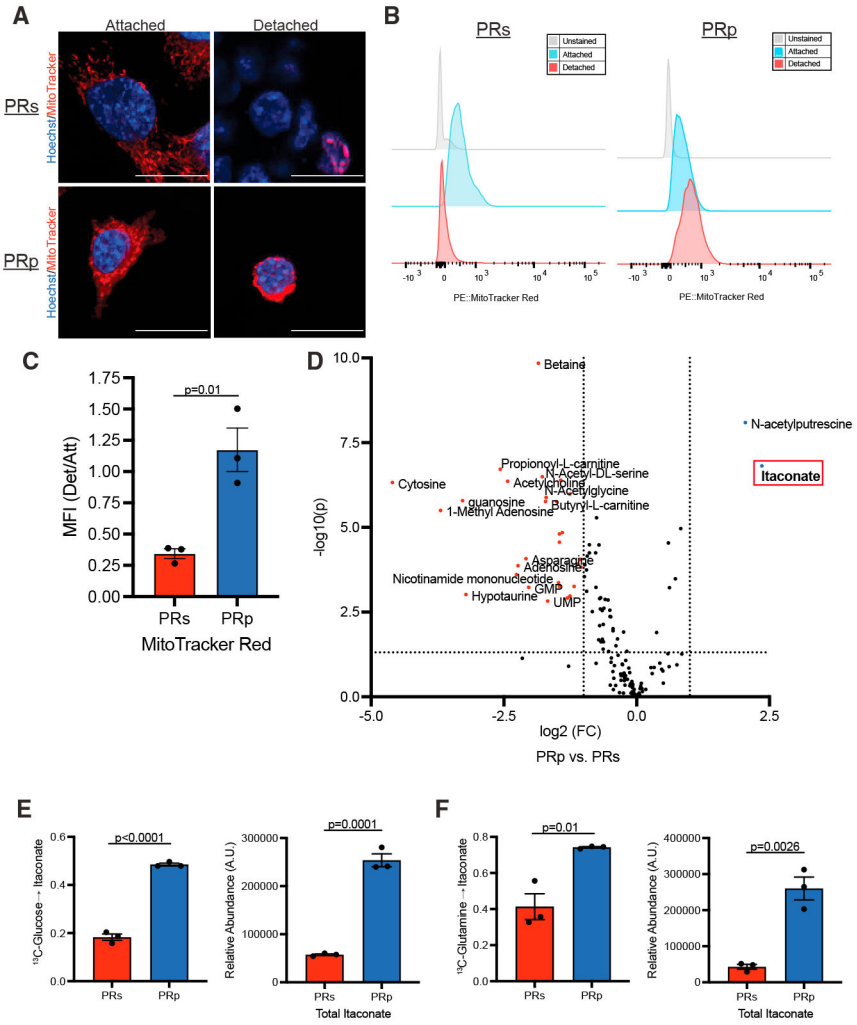

Figure 1. Itaconate (ITA) is produced at high levels in ICB-resistant prostate cancer cells

PRs or PRp cells were grown in the indicated conditions for 24 h. (A) Representative confocal images of cells stained with MitoTracker Red (red) and Hoechst 33342 (blue). Scale bars, 20 μm.

(B and C) Flow cytometry of cells stained with MitoTracker Red. Representative histograms (B) and mean fluorescence intensity (MFI) expressed relative to the corresponding attached (Att) culture condition

(C). n = 3 independent biological samples.

(D) Volcano plot for intracellular metabolites in PRs and PRp cells after 24 h of detachment (Det). $p < 0.05$ and fold change (FC) > 1.2 used for cutoffs.

(E) Fractional enrichment of labeled ITA (left) and total pool (right) from [U-^{13}C]glucose tracing.

(F) Fractional enrichment of labeled ITA (left) and total pool (right) from [U-^{13}C]glutamine tracing. Labeling done for 4 h in detached cells. Graphs represent data collected from a minimum of 3 biological replicates. p values are calculated by two-tailed Student's t test. Data are mean ± SEM.

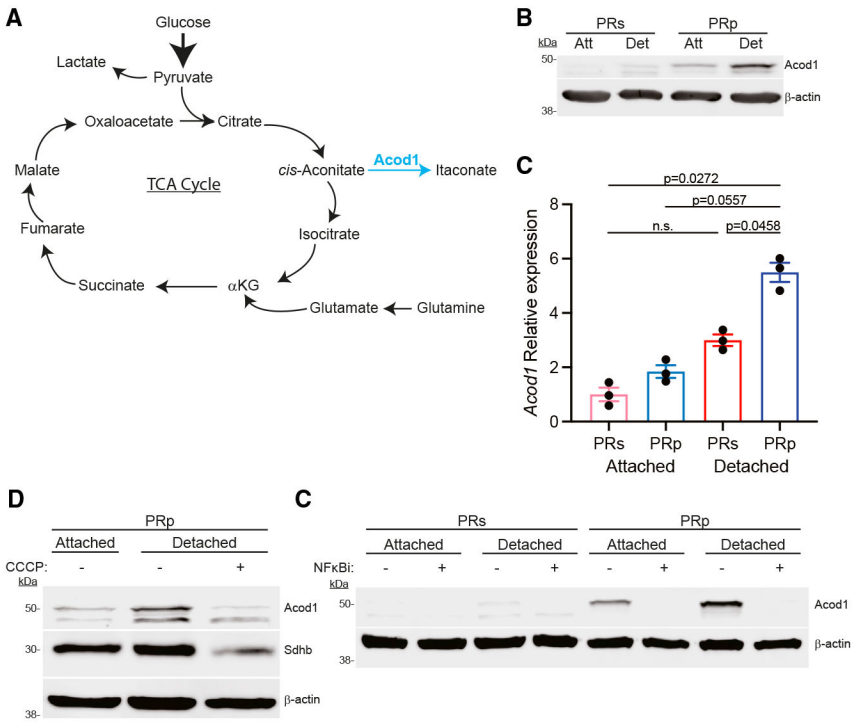

Figure 2. ACOD1 levels are elevated in ICB-resistant cells

(A) Schematic of ITA generation by *cis*-aconitate decarboxylase (Acod1).

(B and C) PRs or PRp cells were grown in the indicated conditions for 24 h.

(B) Lysates were collected and immunoblotted as noted.

(C) Gene expression of *Acod1* by quantitative real-time PCR calculated as FC relative to Att PRs.

(D) PRp cells were grown in the indicated conditions in the presence of DMSO or carbonyl cyanide *m*-chlorophenyl hydrazone (CCCP) (20 μM) for 48 h. Lysates were collected and immunoblotted as noted.

(E) PRs or PRp cells were grown in the indicated conditions in the presence of DMSO or the nuclear factor κB (NF-κB) inhibitor BAY1170-82 (2.5 μM) for 9 h. Lysates were collected and immunoblotted as noted. Graphs represent data collected from a minimum of 3 biological replicates, and all western blotting experiments were independently repeated a minimum of three times with similar results. p values are calculated by one-way ANOVA followed by Tukey's test in (C). Data are mean ± SEM.

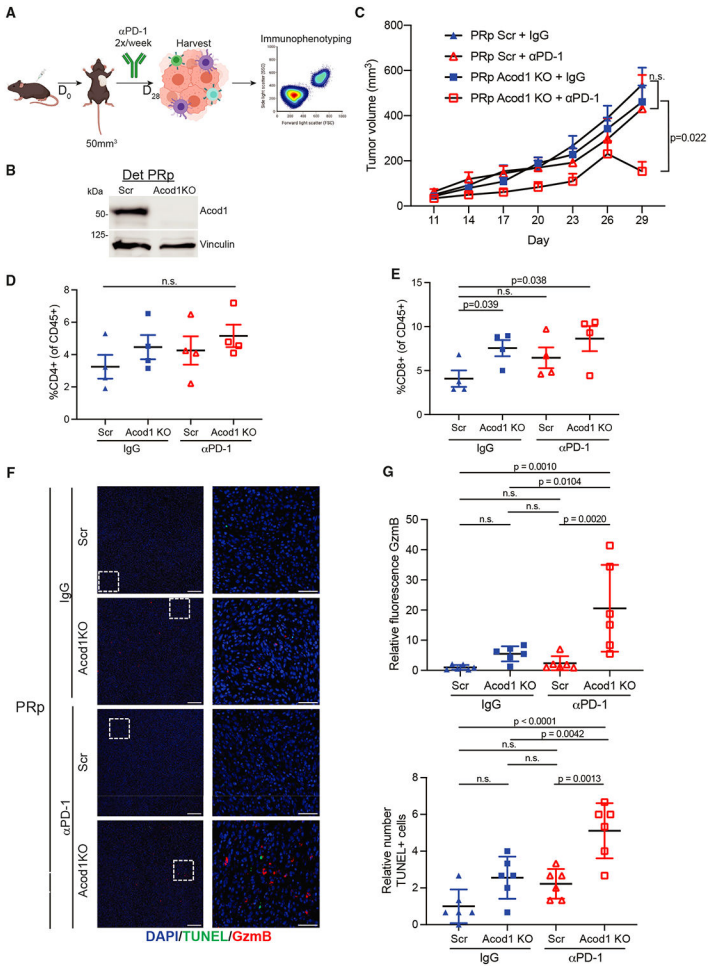

Figure 3. ACOD1 dictates sensitivity to αPD-1 ICB in vivo

(A) Experimental design of *in vivo* experiment.

(B) Western blot for Acod1 of cells injected for tumor experiments.

(C) PRp Scr or PRp Acod1 KO cells were subcutaneously injected in mice and received either isotype control (IgG) or αPD-1 monoclonal antibody (mAb) when tumors reached ≥50 mm^3. Data are mean ± SEM (n = 6–10 per group), and p values were calculated by two-way ANOVA.

(D and E) Percentage of $CD4^+$ (D) or $CD8^+$ (E) T cells within each tumor. Data represent the mean ± SEM (n = 4 mice/group), and p values were calculated by two-tailed Student's t test. n.s., not significant.

(F) Representative images of immunofluorescence (IF) staining of $GzmB^+$ (red) and $TUNEL^+$ (green) cells in tumors from the indicated conditions described in (A). Scale bars of low and high magnification represent 200 and 50 μm, respectively. DAPI, 4′,6-diamidino-2-phenylindole.

(G) Quantification of relative GzmB intensity (top) or average number of $TUNEL^+$ cells (bottom) with SD from six random fields of view (FOVs). The p values were calculated by one-way ANOVA. n.s., not significant.

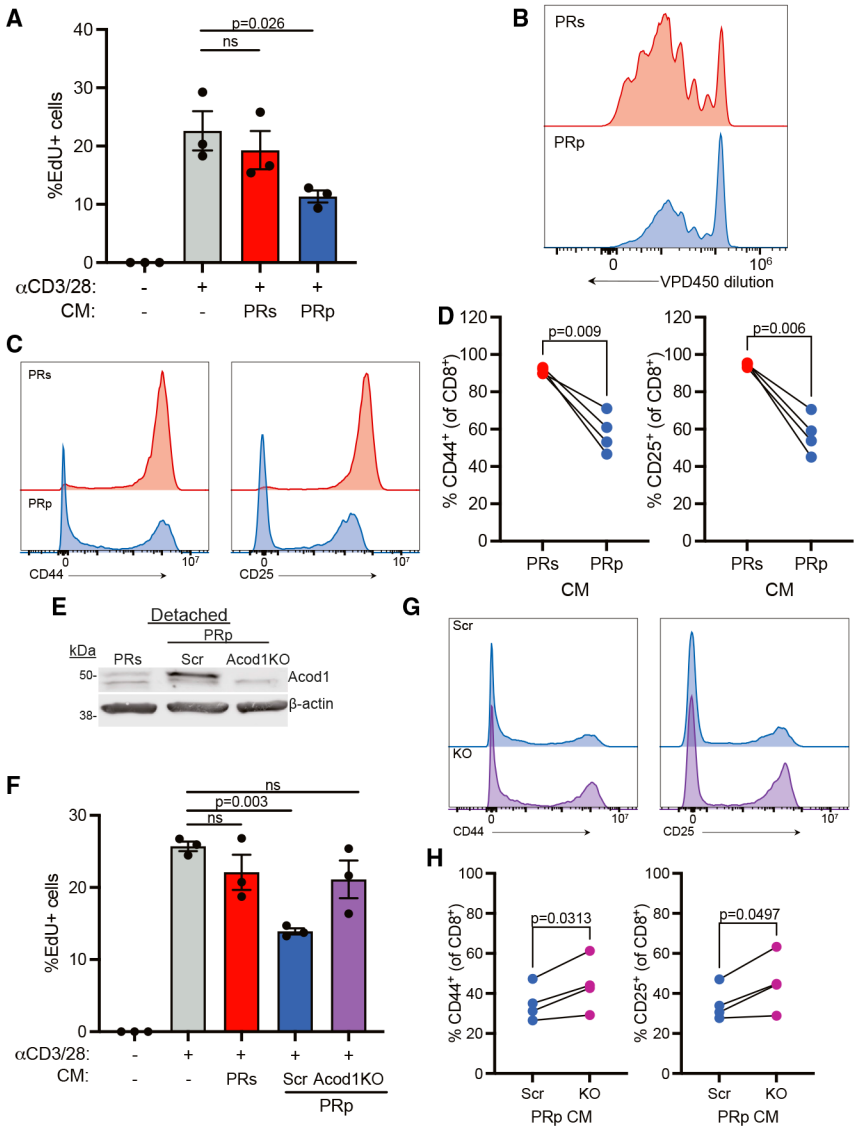

Figure 4. Secreted factors from ECM-Det ACOD1-high cells restrict T cell activation and proliferation

(A) Percentage of EdU$^+$ CD8$^+$ T cells following 48 h of activation with αCD3/CD28 in indicated conditioned medium (CM).

(B) Representative histograms of violet proliferation dye 450 (VPD450) dilution in CD8$^+$ T cells following 72 h of activation with αCD3/CD28 in indicated CM.

(C) Histograms of CD44 (left) and CD25 (right) expression in CD8$^+$ T cells following 72 h of activation with αCD3/CD28 in indicated CM (n = 3).

(D) Percentage of CD44$^+$ (left) and CD25$^+$ (right) CD8$^+$ T cells following 72 h of activation with αCD3/CD28 in indicated CM.

(E) Cells grown for 24 h in Det conditions. Lysates were collected and immunoblotted as noted.

(F) Percentage of EdU$^+$ CD8$^+$ T cells as described in (A).

(G) Histograms of CD44 (left) and CD25 (right) expression as described in (C). Scr, PRp Scr CM; KO, PRp Acod1 KO CM (n = 3).
(H) Percentage of $CD44^+$ (left) and $CD25^+$ (right) $CD8^+$ T cells as described in (D).
Data from EdU experiments (A and F) represent the means ± SEM of triplicate wells, and p values were calculated by one-way ANOVA analysis. Data are representative of three independent experiments. The p values for the T cell activation experiments (D and H) were calculated using a paired, two-tailed t test (n = 4 mice/group). n.s., not significant. Western blotting and VPD450 dilution experiments were independently repeated a minimum of three times with similar results.

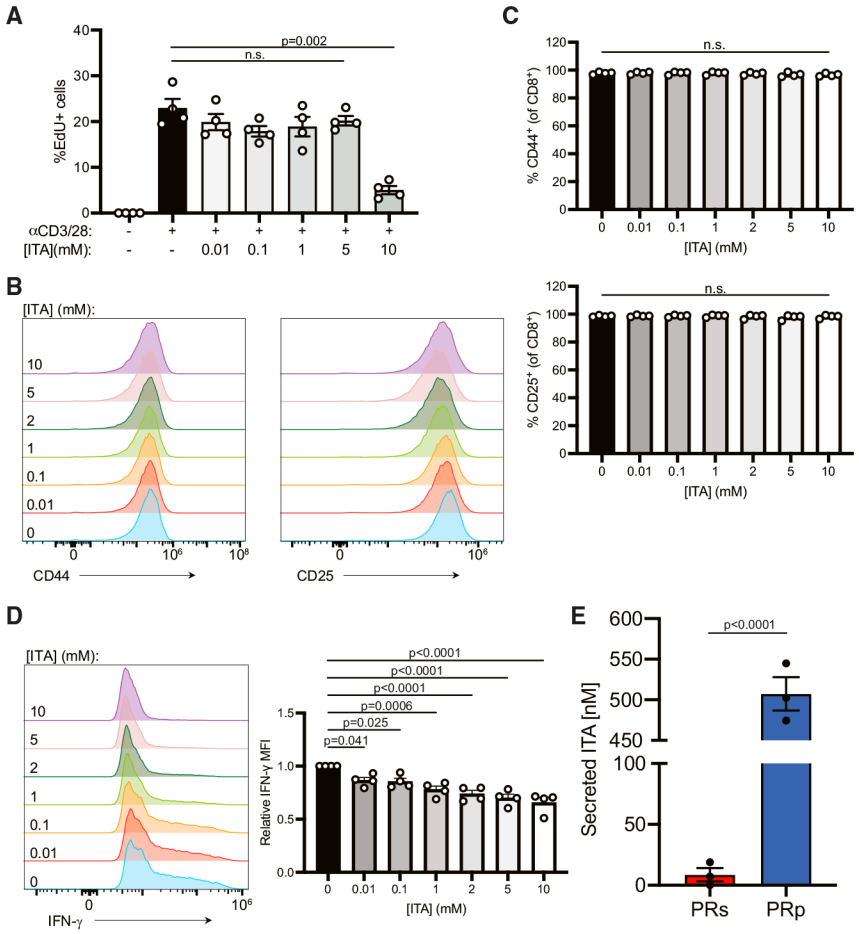

Figure 5. ACODI-mediated effect on CD8$^+$ T cells is independent of extracellular ITA

(A) Percentage of EdU+ CD8$^+$ T cells following 48 h of activation with αCD3/CD28 in the presence of the indicated concentrations of ITA.

(B) Histograms of CD44 (left) and CD25 (right) expression in CD8$^+$ T cells following 72 h of activation with αCD3/CD28 in the presence of the indicated concentrations of ITA.

(C) Bar graphs showing the percentage of CD44$^+$ (top) or CD25$^+$ (bottom) CD8$^+$ T cells activated as described in (B).

(D) IFN-γ production by CD8$^+$ T cells activated as in (B). Representative histograms of IFN-γ expression in CD8$^+$ T cells (left) and relative MFI of IFN-γ in IFN-γ$^+$ CD8$^+$ T cells (right).

(E) Concentration of ITA in the CM from PRs or PRp cells.

Data in EdU experiment (A) represent the means ± SEM of four replicate wells. Data are representative of three independent experiments. Data in (C) and (D) represent the means ± SEM (n = 4 mice/group). One-way ANOVA analysis. Data in (E) are analyzed by two-tailed Student's t test. n.s., not significant.

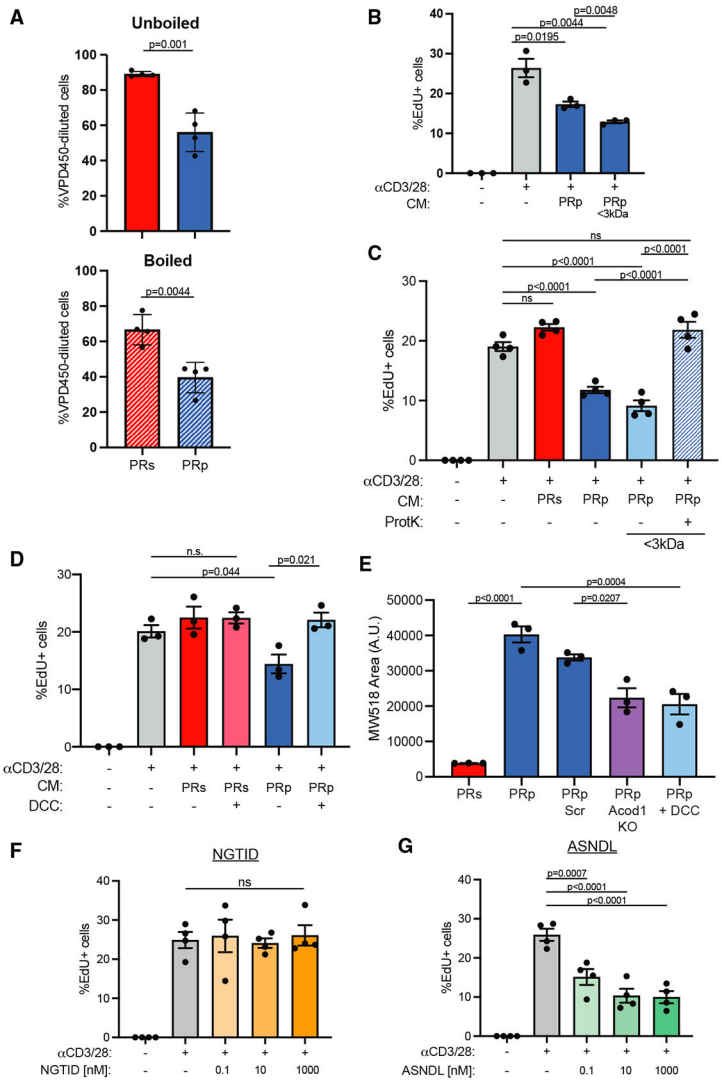

Figure 6. ACOD1 regulates the secretion of immunomodulatory peptides

(A) VPD450 dilution in $CD8^+$ T cells following 72 h of activation with αCD3/C28 in indicated CM that was either not boiled (top) or boiled (bottom) prior to activating the T cells.

(B) Percentage of EdU^+ $CD8^+$ T cells following 48 h of activation with αCD3/C28 in full PRp CM or <3 kDa fraction of PRp CM.

(C and D) Percentage of EdU^+ $CD8^+$ T cells in indicated conditions following activation as noted in (B).

(E) Bar graph showing the relative abundance of a 518 Da molecular weight compound in the listed CM.

(F and G) Percentage of EdU^+CD8^+T cells following 48 h of activation in the presence of either NGTID peptide (F) or ASNDL peptide (G). Peptides were used at 0.1, 10, or 1,000 nM.

Data in (A) represent the mean ± SEM (n = 4 mice/group). Data in EdU experiments (B–D, F, and G) represent the means ± SEM of four replicate wells. Data are representative of

three independent experiments. p values were calculated by two-tailed Student's t tests (A) or one-way ANOVA analysis (B–G). n.s., not significant.

KEY RESOURCES TABLE

REAGENT or RESOURCE	SOURCE	IDENTIFIER
Antibodies		
Mouse monoclonal anti-β-actin	Sigma-Aldrich	A1978; RRID: AB_476692
Rabbit monoclonal anti-Tom20	Cell Signaling	#42406; RRID: AB_2687663
Rabbit polyclonal anti-mouse Irg1/Acod1	Cell Signaling	#17805; RRID: AB_3064865
Rabbit monoclonal anti-human IRG1/ACOD1	Cell Signaling	#77510; RRID: AB_2799901
Rabbit monoclonal anti-GzmB	Cell Signaling	#44153; RRID: AB_2857976
Mouse monoclonal anti-Tim23	BD Biosciences	611222; RRID: AB_398754
Rabbit polyclonal anti-Sdhb	Proteintech	10620-1-AP; RRID: AB_2285522
Mouse monoclonal anti-Vinculin	Proteintech	66305-1-Ig; RRID: AB_2810300
Rat monoclonal anti-mouse CD45-FITC	Tonbo Biosciences	Clone 30-F11; RRID: AB_2621689
Rat monoclonal anti-mouse CD4-APC	Tonbo Biosciences	Clone GK1.5; RRID: AB_2621543
Rat monoclonal anti-mouse CD8-PE	Tonbo Biosciences	Clone 2.43; RRID: AB_2621788
Rat monoclonal anti-mouse CD16/32	BioLegend	Clone 93; RRID: AB_312800
Rat monoclonal anti-mouse CD279 (PD-1)	BioLegend	Clone RMP1-14; RRID: AB_2566090
Rat monoclonal IgG2a	BioLegend	Clone RTK2758; RRID: AB_2819062
Goat anti-rabbit IgG Alexa Fluor 647	Thermo Fisher	A-21245; RRID: AB_2535813
Donkey anti-mouse IgG Alexa Fluor+ 680	Thermo Fisher	A32788; RRID: AB_2762831
Donkey anti-rabbit IgG Alexa Fluor+ 800	Thermo Fisher	A32808; RRID: AB_2762837
Hamster monoclonal anti-mouse CD3e	eBioscience	Clone 145-2C11; RRID: AB_467051
Hamster monoclonal anti-mouse CD28	eBioscience	Clone 37.51; RRID: AB_467192
Rat monoclonal anti-mouse CD8a-BUV395	BD Biosciences	Clone 53.67; RRID: AB_2732919
Rat monoclonal anti-mouse CD44-BUV805	BD Biosciences	Clone IM7; RRID: AB_2871234
Rat monoclonal anti-mouse CD4-BV605	BioLegend	Clone RM4-5; RRID: AB_11125962
Rat monoclonal anti-mouse CD25-488	eBioscience	Clone PC61.5; RRID: AB_763472
Rat monoclonal anti-mouse IFN-gamma-APC	eBioscience	Clone XMG1.2; RRID: AB_469504
Mouse monoclonal anti-GzmB-PE	BioLegend	Clone QA16A02; RRID: AB_2687031
Chemicals, peptides, and recombinant proteins		
DMEM with 4.5 g/L with glucose and L-glutamine, without sodium pyruvate	Gibco	12100–046
RPMI-1640 with L-glutamine	Gibco	31800–022
McCoy's 5A Medium	Gibco	16600–082
IMDM	Wisent Inc.	319-105-CL
2-mercaptoethanol	Gibco	21985023
Poly-HEMA	Sigma-Aldrich	P3932
D-Glucose [$^{13}C_6$]	Cambridge Isotopes	CLM-1396
L-Glutamine [$^{13}C_5$]	Cambridge Isotopes	CLM-1822
D-Glucose	Sigma-Aldrich	G7021
L-Glutamine	Sigma-Aldrich	49419
Itaconate	Sigma-Aldrich	I29204
MitoTracker Red CM-H_2XRos	Invitrogen	M7513

REAGENT or RESOURCE	SOURCE	IDENTIFIER
Hoechst 33342	Invitrogen	H1399
DAPI	Invitrogen	D3571
BAY1170-82	Sigma-Aldrich	B5556
ACK Lysis Buffer	Gibco	A1049201
Foxp3/Transcription factor staining buffer set	eBioscience	00-5523-00
Nu-Serum IV Culture Supplement	Corning	355504
Phorbol 12-myristate 13-acetate (PMA)	Sigma-Aldrich	P-8139
Ionomycin	Sigma-Aldrich	10634
BD GolgiStop	BD Biosciences	51-2092KZ
Violet Proliferation Dye 450	BD Biosciences	562158
Fixable Viability Dye eFluor 780	eBioscience	65-0865-14
Dextran coated charcoal (DCC)	Sigma-Aldrich	C6241
Proteinase K	Sigma-Aldrich	P2308
SignalStain Citrate Unmasking Solution	Cell Signaling	14746
Collagenase IV	Invitrogen	17104019
Live/Dead Aqua 405	Invitrogen	L34966
NGTID peptide	This paper	N/A
ASNDL peptide	This paper	N/A
Lipofectamine 2000 transfection reagent	Invitrogen	11668019
Carbonyl cyanide 3-chlorophenylhydrazone (CCCP)	Sigma-Aldrich	C2759
Normal Goat Serum	Life Technologies	500622
ProLong Gold Antifade	Invitrogen	P36934
Low-melt agarose	Invitrogen	16520050
Iodonitrotetrazolium formazan (INT-Violet)	Sigma-Aldrich	58030
Critical commercial assays		
Zymo Quick RNA Miniprep kit	Zymo Research	R1054
Click-iT EdU kit	Thermo Fisher	C10340
In Situ Cell Death Detection Kit, TMR Red	Roche	#12156792910
Mouse naive $CD8^+$ T cell isolation kit	Miltenyi Biotec	130-096-543
Dynabeads mouse αCD3/28	Thermo Fisher	11452D
EasySep mouse naive $CD8^+$ T cell isolation kit	Stem Cell Technologies	19858A
Deposited data		
Metabolomics raw data	This paper	MassIVE (ProteomeXchange) Accession number: PXD050289
Experimental models: Cell lines		
PRs cells	Xin Lu	Murphy et al.[34]
PRp cells	Xin Lu	Murphy et al.[34]
293T cells	ATCC	CRL-3216
DU145 cells	Jianneng Li	RRID: CVCL_0105
MDA-MB-436 cells	ATCC	HTB-130
PC3 cells	ATCC	CRL-1435

REAGENT or RESOURCE	SOURCE	IDENTIFIER
GCT cells	ATCC	TIB-223
Experimental models: Organisms/strains		
C57BL/6N mice	Envigo	4405
C67BL/6J mice	Jackson Laboratories	JAX:000664
Oligonucleotides		
gRNA 1 (pLV-hCas9 backbone): GGGCTTCCGATAGAGCTGTG	This paper	N/A
gRNA 2 (pLV-hCas9 backbone): AACGTTGGTATTGAAGTACA	This paper	N/A
Scramble gRNA (pLV-hCas9 backbone): GTGTAGTTCGACCATTCGTG	VectorBuilder	VB010000-9355sqw
Primer 18S Forward: GGCGCCCCCTCGATGCTCTTAG	This paper	N/A
Primer 18S Reverse: GCTCGGGCCTGCTTTGAACACTCT	This paper	N/A
Primer for mouse Acod1 Forward: GCAACATGATGCTCAAGTCTG	This paper	N/A
Primer for mouse Acod1 Reverse: TGCTCCTCCGAATGATACCA	This paper	N/A
Recombinant DNA		
pLV-hCas9	VectorBuilder	This paper
psPAX2	Addgene	Plasmid #12260
pCMV-VSV-G	Addgene	Plasmid #6454
Software and algorithms		
Compound Discoverer (v 3.3)	Thermo Scientific	https://www.thermofisher.com/us/en/home.html
FlowJo v9.9.5	FlowJo LLC	https://www.flowjo.com
GraphPad Prism v9	GraphPad Software	https://www.graphpad.com/
ImageJ, version 1.52a for Mac	National Institutes of Health	https://imagej.net/ij/index.html